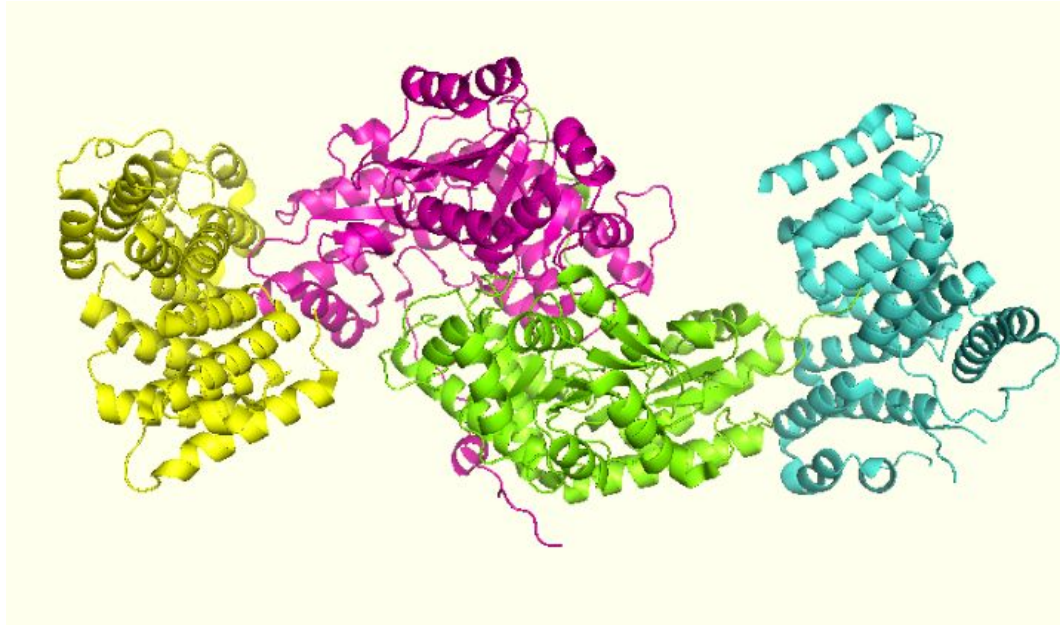


CHALMERS



Investigation of the Cargo Recognition Step in Peroxisomal Import

Master of Science Thesis in Chemistry and Bioscience

YE LOU

Department of Chemical and Biological Engineering
CHALMERS UNIVERSITY OF TECHNOLOGY
Göteborg, Sweden, 2011

Investigation of the cargo recognition step in peroxisomal import

© Ye Lou, 2011

Department of Chemical and Biological Engineering

Chalmers University of Technology

41296 Gothenburg

Sweden

Supervisor: Dr. Krisztian Fodor

European Molecular Biology Laboratory, Hamburg Outstation

22603 Hamburg

Germany

Examiner: Prof. Joakim Norbeck

Department of Chemical and Biological Engineering

Chalmers University of Technology

41296 Gothenburg

Sweden

Abstract

Peroxisomes are cellular organelles present in all eukaryotic cells, which contain enzymes that catalyze certain oxidative reactions and metabolic processes. Proteins are selectively imported across the membrane into the peroxisomal lumen in their folded and active form. Peroxin 5 (Pex5p) is a cycling receptor responsible for the translocation of matrix proteins equipped with a type 1 peroxisome targeting signal (PTS1). The PTS1 is usually a conserved C-terminal tripeptide (S/A/C–K/R/H–L/M) which interacts with the TPR domain of Pex5p.

In order to get a better understanding of the recognition step of the Pex5p import cycle, two model proteins were used: human alanine-glyoxylate aminotransferase (AGT) and human Peroxiredoxin 5 (PRDX5).

Although Pex5p-dependent, human AGT has a unique, non-consensus PTS1: - KKL. Six mutants (Q385A, P388A, K389A, K390A, K391A and K390A/K391A) were constructed, which are localized not only within the C-terminal tripeptide, but also in the immediate upstream region. According to the circular dichroism and enzyme activity measurements, the conformation of the mutants did not change and they were fully active when bound to Pex5p. The isothermal titration microcalorimetry (ITC) experiment of the K390A demonstrated a binding affinity 10 times higher than that of the wildtype AGT. And the ITC experiment as well as the GST-pull down assay revealed that the K391A mutant was unable to interact with Pex5p. The structure of K390A-Pex5p (TPR) complex was solved by X-ray crystallography, from which we noticed a significant shift of the Pex5p TPR domain's position compared to the wildtype complex. The data indicates that the structural flexibility of the receptor molecule allows sufficient binding of cargoes with various PTS1s.

PRDX5 has a canonic PTS1 at its C-terminus: -SQL. However, there is no binding to the Pex5p receptor under laboratory conditions. To free up the PTS1, the N142A, Q161K and N142A/C47S/C151S/N157A mutants were constructed, and their interactions with Pex5p were tested by GST-pull down and ITC. As a result, Q161K was observed to interact with Pex5p, which was confirmed by analytical size exclusion chromatography coupled with static light scattering. An ITC dilution assay of Q161K revealed a critical transition concentration in the very low micromolar range. The rather abrupt transition indicates that the dimerization occurs only above the critical transition concentration when there are enough monomers in the solution to trigger it. It is also suggested that the monomer form of PRDX5 binds Pex5p.

Key words: Cargo recognition; PTS1; Peroxisomal translocation; AGT; PRDX5.

Abbreviation

AGT – alanine-glyoxylate aminotransferase
BSA – bovine serum albumin
BME – β -mercaptoethanol
CD – circular dichroism
DTT – dithiothreitol
FPLC – Fast protein liquid chromatography
GF – gel filtration
GST – glutathione S transferase
HEPES – 4-(2-Hydroxyethyl)-1-piperazineethanesulfonic acid
ITC – isothermal titration calorimetry
IPTG – isopropyl-beta-D-thiogalactopyranoside
L – liter
LB – Luria Bertani
LIC – ligase independent cloning
LDH – lactate dehydrogenase
M – mole
mM – milimole
mg – milligram
min – minute
ml – milliliter
MWCO – molecular weight cutoff
NADH – nicotinamide adenine dinucleotide
OD – optical density
PTS – peroxisome targeting sequence
Pexp – peroxin protein
PLP – pyridoxal 5-phosphate
PEG – polyethylene glycol
PCR – polymerase chain reaction
PH1– primary hyperoxaluria type 1
PRDX5 – peroxiredoxin 5
rpm – revolutions per minute
SCP2 – sterol carrier protein 2
SOC – super optimal broth with catabolic repressor
SDS-PAGE – sodium dodecyl sulfate polyacrylamide gel electrophoresis
SLS – static light scattering
TB – terrific broth
Tris – tris (hydroxymethyl) aminomethane
TPR – tetratricopeptide repeat
 μ g – microgram
 μ l – microliter
 μ m – micrometer

Table of Content

Part A Human alanine-glyoxylate aminotransferase

Introduction	1
1. Peroxisome.....	1
2. Matrix protein translocation into peroxisomes	1
2.1 Cargo recognition step and targeting	2
2.2 Molecular mechanisms of Pex5p-dependent uimport.....	2
3. Human alanine-glyoxylate Aminotransferase (AGT).....	4
3.1 Non consensus PTS1 of human AGT	5
3.2 Crystal structure of Pex5p-human AGT complex.....	6
Materials and Methods	8
1. AGT mutants preparation	8
1.1 Ligase independent cloning (LIC) of K389A	8
1.2 Transformation	12
1.3 Protein Expression	12
1.4 Purification.....	12
2. Pex5p (TPR domain) preparation	13
3. Glutathione S-Transferase (GST) pull down assay	14
4. Enzyme Activity Measurement.....	15
5. Circular dichroism (CD) measurement.....	16
6. Isothermal Titration Calorimetry (ITC) experiment.....	16
7. Crystallization of K390A-Pex5p & K390A/K391A-Pex5p complex.....	16
8. Data collection and structure determination	17
Results	18
1. K389A mutant construction.....	18
2. Purification of AGT mutants	19
3. GST pull down.....	21
4. Enzyme activity measurement	22
5. CD measurement.....	23
6. ITC experiment.....	24
7. Crystallization of K390A-Pex5p (TPR) & K390A/K391A-Pex5p (TPR) complex, data collection and structure determination	27
Discussion	31
Reference	33

Part B Human Peroxiredoxin 5

Introduction	36
1. PRDX5 and its structure	36
2. PTS1 of human PRDX5	37
Materials and Methods	39
1. Quick change mutagenesis	39
2. Over expression and purification	40
3. GST-pull down	40
4. Size exclusion chromatography coupled with static light scattering	40
5. High-throughput crystallization of the Pex5p-Q161K complex	41
6. ITC experiments	41
Results	42
1. Quick change mutagenesis	42
2. GST pull down	42
3. SLS experiment	43
4. ITC experiment	45
5. High-throughput screening of crystallization condition	48
Discussion	49
Reference	50
Conclusion	51
Appendix I Buffers and solutions	I
Appendix II ITC figures	II

Part A

**Human alanine-glyoxylate
aminotransferase**

Introduction

1. Peroxisome

Peroxisomes (also called microbodies) are organelles found in almost all eukaryotic cells (Veenhui *et al*, 2002). In humans, the function of peroxisomes is primarily to catalyze fatty acid beta-oxidation, particularly of long chain fatty acids, breaking them down into acetyl CoA. They will then be transported via the cytosol to the mitochondria to feed the TCA cycle or to be used for biosynthetic reactions. In addition, peroxisomes catalyze detoxification reactions, like the degradation of the metabolic byproduct hydrogen peroxide (Purdue and Lazarow, 2001). This normally happens in the liver and kidney cells. The functional versatility of peroxisomes allows the cells to adapt to developmental or varying environmental conditions.

2. Matrix protein translocation into peroxisomes

Proteins destined for the peroxisome matrix are synthesized in the cytosol (Lazarow and Fujiki, 1985), followed by translocation with the help of many peroxins in the peroxisome membrane and the cytosol (Fig.1). Peroxins are proteins mediating the import of peroxisomal integral membrane and matrix proteins, and they are necessary for peroxisome biogenesis.

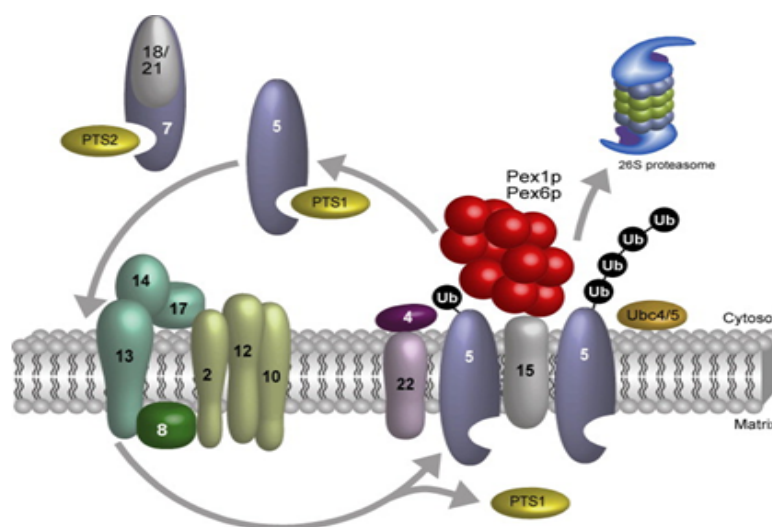


Fig.1 Peroxisomal matrix protein import cascade (Platta and Erdmann, 2004)

2.1 Cargo recognition step and targeting

Protein targeting to the peroxisome is signal dependent, most of them depends on either of the two targeting signals, PTS1 or PTS2, which are recognized by the cytosolic receptors Pex5p and Pex7p, respectively. The receptor/cargo complex first interacts with the docking subcomplex at peroxisomal membrane. The docking subcomplex is composed of Pex13p, Pex14p and Pex17p (in yeast), which contacts with the RING subcomplex (Pex2p, Pex10p, Pex12p) by Pex8p or Pex3p to form a larger complex called the importomer. Pex3p also interacts with another protein called Pex19p. After import into the peroxisome, the cargo proteins release from receptors into the peroxisome matrix, while the receptors undergo a recycling to cytosol (Holroyd and Erdmann, 2001). The Pex8p may promote the dissociation of the Pex5p–PTS1 cargo complex, and might be playing an important role in cargo release (Wang *et al.*, 2003). There exists a peroxisomal quality control pathway which involves ubiquitination of improperly recycled Pex5p to protease degradation (Erdmann *et al.*, 2004 and Kiel *et al.*, 2005).

2.2 Molecular mechanisms of Pex5p-dependent uimport

2.2.1 Peroxisome targeting signal (PTS1)

As mentioned above, the import of peroxisomal proteins depends on Pex5p or Pex7p, and they can be translocated in their folded and active form. The majority of peroxisomal proteins contain a Peroxisome Targeting Signal (PTS1) in the extreme C terminus, which interacts with the principal peroxin Pex5p as receptor (Gould *et al.*, 1989 and Lametschwandtner *et al.*, 1998). It differs from the mechanisms of transport into the mitochondria or chloroplasts where the targeting signal locates at the amino-terminus.

A typical PTS1 consists of three amino acids, Serine–Lysine–Leucine (-SKL) and its variants thereof (Gould *et al.*, 1989). A refined PTS1 motif definition is that the first position contains a small uncharged side chain (S/A/C), at the penultimate position a positively charged residue (K/R/H) and at the extreme C-terminal position a leucine or methionine (Subramani *et al.*, 1992). However, it has been found that the presence of the consensus tripeptide may not be sufficient for peroxisomal targeting (Brocard *et al.*, 2006). Some previous studies show that apart from the known C-terminal tripeptide, at least nine residues directly upstream are also important for signal recognition in the PTS1–Pex5 receptor complex (Neuberger *et al.*, 2003). Moreover, in some specific cases, there may be a second contact region in the matrix protein structure, accounting for the stability of the interaction and consequently for the efficiency of import (Huber *et al.*, 2005).

A wide range of Pex5p-PTS1 peptide affinities using the PTS1 peptides from peroxisomal proteins of the human proteome has been reported (Ghosh and Berg, 2010). It demonstrated that the PTS1s of some proteins have substantially higher affinities to Pex5p than others, the dissociation constant of them range from 1.6nM of acyl-CoA oxidase 3 to 26mM of hydroxyacid oxidase 1 (HAO1). It appears that these PTS1 sequences and gene expression levels may have evolved to provide a relatively uniform population of Pex5p-cargo complexes.

2.2.2 Peroxin5

Peroxin5 (Pex5p, P50542) is a 71 kDa protein, composed of two domains. The N-terminal part is mainly unfolded, and has a role in the docking to the peroxisomal membrane. The C-terminal domain is globular and mainly composed of tetratricopeptide repeats (TPRs). TPRs are helix-turn-helix motifs, tandemly repeated to generate regular α -solenoid proteins with a generalised function in protein-protein interactions. In Pex5p, the TPR domain interacts directly with the PTS1, after which the cargo is targeted into peroxisomal lumen (Brocard *et al*, 1994).

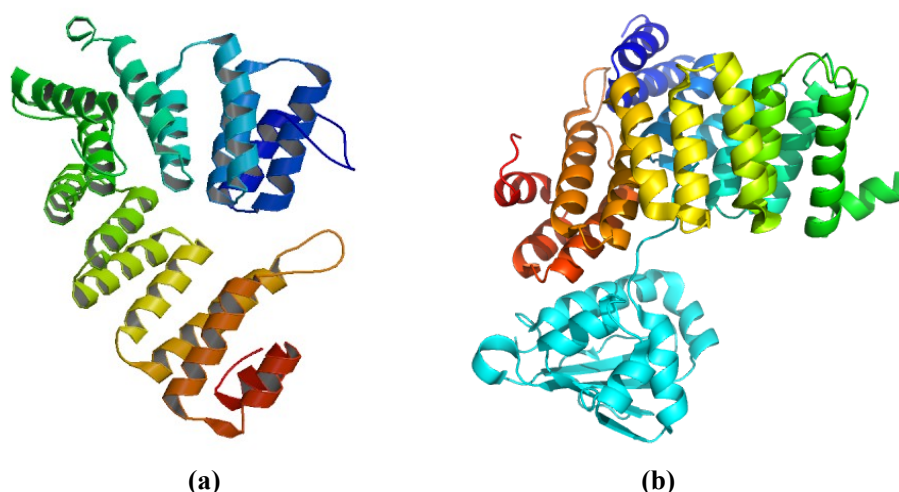


Fig.2 The Crystal structures of the Pex5p TPR domain in the presence and absence of cargo
(a) open and snail-like structure (b) close and circular structure when interacting with SCP2

In the previous studies of Pex5p, it was found that the conformation changed from an open snail-like structure to a close circular conformation, when the model cargo protein sterol carrier protein 2 (SCP2) was loaded (Fig.2) (Stanley *et al*, 2006). It was mainly caused by a long loop C terminal to the 7-fold tetratricopeptide repeat segments (Fig 3, Stanley and William, 2010).

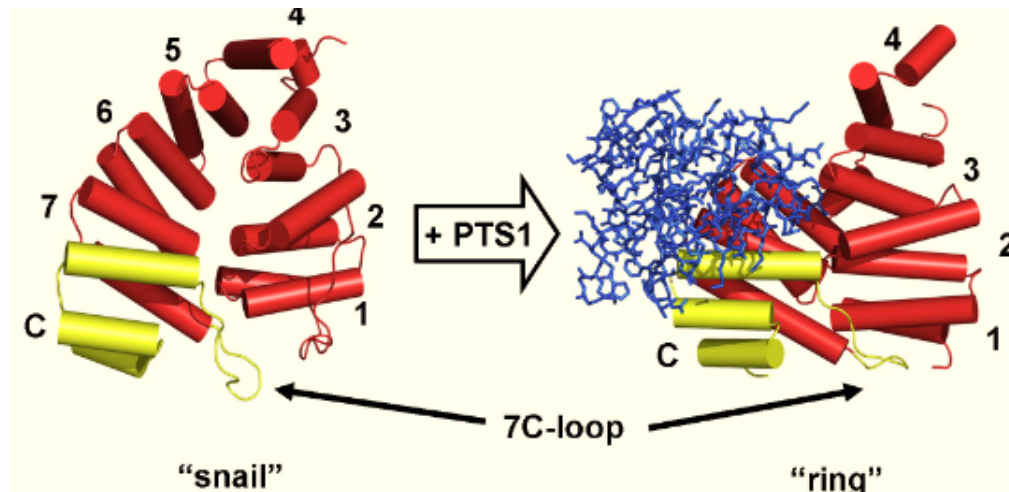
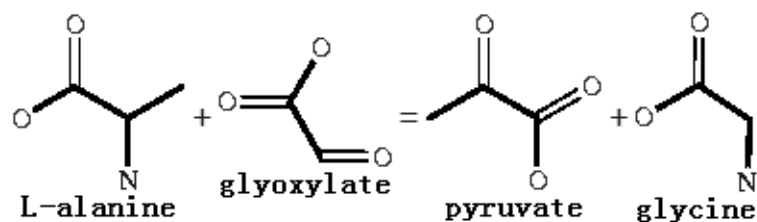


Fig.3 Conformation change of Pex5p C-terminus (Stanley *et al*, 2006)

It is still under debate how cargo proteins are imported into peroxisomes across the peroxisomal membrane with the help of Pex5p. One hypothesis is that Pex5p enters the peroxisome together with a loaded cargo, known as the extended-shuttle model. The Pex5p-PTS1 complex first interacts with the docking subcomplex (Pex13p, Pex14p and Pex17p), followed by translocation via the docking subcomplex into the peroxisome matrix where Pex5p would interact with Pex8p, and then with the RING subcomplex (Pex2p, Pex10p, Pex12p) during their return back to the cytosol (Subramani *et al*. 2006). Some other studies support another model of cargo translocation. It was revealed that Pex5p can behave like an integral membrane protein (Azevedo *et al*, 2000). There is a “transient pore model” describing that the oligomeric Pex5p assembled to form a pore at peroxisome membrane, through which cargoes entered into peroxisome matrix. After that, the pore disassembled and Pex5p recycled to the cytosol for another round of cargo import (Erdmann and Schliebs, 2005).

3. Human alanine-glyoxylate Aminotransferase (AGT)

Alanine-glyoxylate aminotransferase (AGT, P21549) is a peroxisomal pyridoxal 5-phosphate (PLP, Fig.4) dependent enzyme that catalyzes the chemical reaction:



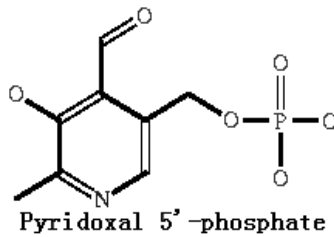


Fig.4 PLP structure

Human AGT contains 392 amino acids, and its molecular weight is 43 kDa. In general, AGT forms a homodimer, with one PLP molecule/AGT monomer as a co-factor responsible for catalytic activity (Fig.5). The deficiency of AGT leads to hereditary kidney stone disease primary hyperoxaluria type 1 (PH1). In this case, glyoxylate is metabolized to oxalate, either in peroxisomes by the enzyme glyoxylate oxidase or by lactate dehydrogenase (LDH) after diffusion into the cytosol, and consequently causes deposition of insoluble calcium oxalate in the kidney and urinary tract (Danpure, 1993).

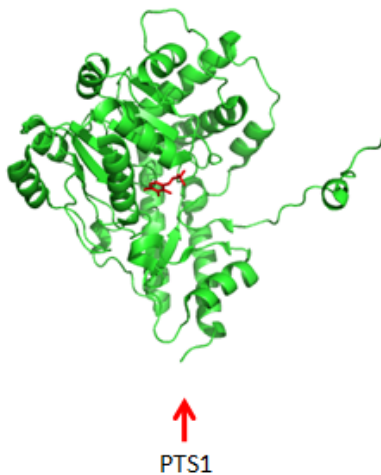


Fig.5 Structure of human AGT monomer. The molecule in red is the PLP as cofactor.

3.1 Non consensus PTS1 of human AGT

Although human AGT is imported into peroxisomes by the Pex5p-dependent pathway, its C-terminal tripeptide (-KKL) is unlike those of any other PTS1s. According to some studies, this unusual PTS1 is necessary for peroxisomal targeting of human AGT, but insufficient to direct the peroxisomal targeting of other reporter proteins by Pex5p (Motley *et al*, 1995), such as bacterial chloramphenicol acetyltransferase or firefly luciferase, which reveals a potential second interaction region in the quaternary structure (Huber *et al*, 2005). This was supported by the phenomenon that Pex5p did not interact with human AGT in yeast two-hybrid assay (Lametschwandtnner *et al*, 1998). Besides, KKL is a unique PTS1 found only in human AGT. However, what

makes it more complicated is that human AGT can be targeted to peroxisomes by all other types of PTS1s found in mammalian AGT except for KKL, like NKL, SQL, HRL and SKL as well (Motley *et al.*, 1995). Furthermore, it was found that the PTS1 peptide of human AGT has very weak binding affinity to Pex5p compared to other human peroxisomal proteins with consensus PTS1 (Ghosh and Berg, 2010). It is hard to understand the reason why human AGT chooses such an abnormal KKL sequence as PTS1.

3.2 Crystal structure of Pex5p-human AGT complex

Despite of the weak binding, the Pex5p (TPR domain)-human AGT complex was crystallized (0.1M Bis-Tris pH 5.3, 0.15M LiSO₄, 17% PEG3350) and its structure has been solved at resolution 2.35 Å as shown in Fig 6 (PDB code: 3R9A). Each subunit of AGT dimer binds to one Pex5p, with the C-terminal PTS1 motif penetrates into the central tunnel of Pex5p (Fig.7(a)).

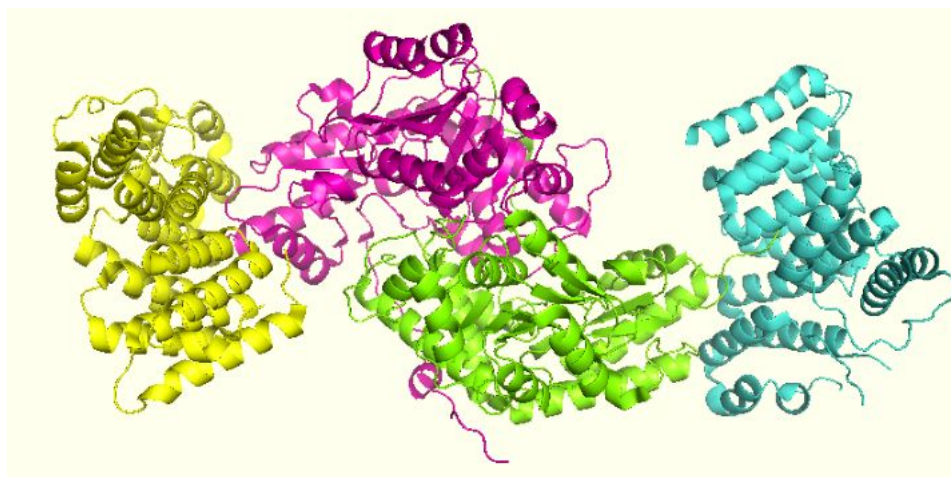
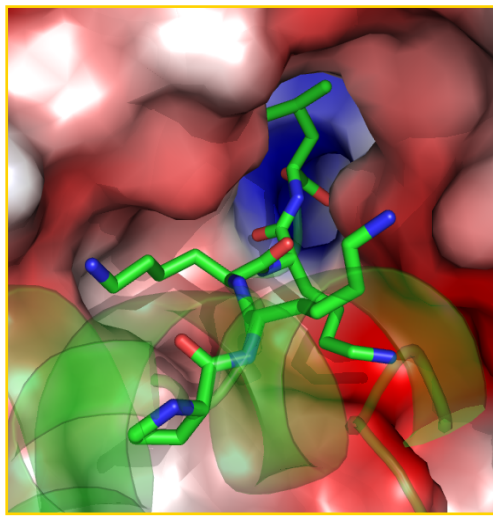
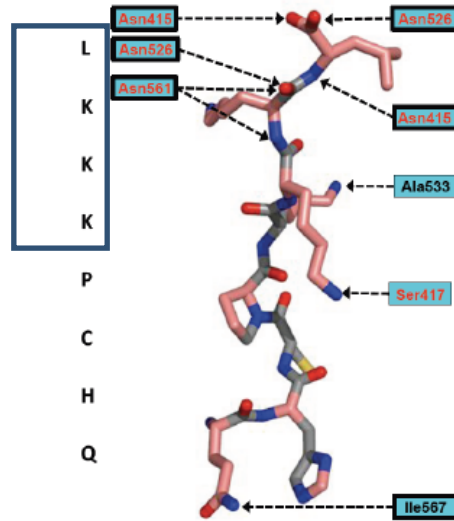


Fig.6. 3D structure of human AGT-Pex5p (TPR) complex. The chains in pink and green are representing the AGT dimer, the ones in yellow and blue are the Pex5p TPR domain



(a)



(b)

Fig.7 Interaction of human AGT PTS1 with Pex5p (Fodor, unpublished). (a) PTS1 inserts into Pex5p central tunnel; (b) The interface of PTS1 region and Pex5p.

For the cargo proteins, it appears that not only the C-terminal tripeptide but also certain upstream amino acids are important for Pex5p recognition as mentioned in 2.2.1. Fig.7(b) shows the interface of human AGT's PTS1 region and Pex5p, from which it can be seen clearly that in addition to the KKL tripeptide, K389 and Q385 form hydrogen bonds to certain residues of Pex5p. However, it is particularly interesting that the lysine 390, a large and positive charged residue, which locates at the -2 position within the PTS1 tripeptide, does not interact directly with Pex5p.

The aim of this project is to better understand the interaction of the non-consensus PTS1 of human AGT with Pex5p, using biochemical and biophysical methods to study the properties and binding affinities of six AGT mutants: Q385A, P388A, K389A, K390A, K391A and K390A/K391A.

Materials and Methods

1. AGT mutants preparation

1.1 Ligase independent cloning (LIC) of K389A

LIC is a fast and simple method to produce expression constructs. It makes use of 3' to 5' activity of T4 DNA polymerase to create very specific 10-15 base single overhangs in the expression vector. PCR products with complementary overhangs are created by building appropriate extensions into the primers and treating them with T4 DNA polymerase as well. The annealing of the insert and the vector is performed in the absence of ligase by simple mixing of the DNA fragments.

1.1.1 Mutagenesis by PCR

Most of the AGT mutant plasmids (Q385A, P388A, K390A, K391A and K390A/K391A) were prepared by other colleagues in the laboratory and were ready for transformation, except K389A.

To make the K389A mutant from wildtype AGT in pETM-30 vector, the forward and reverse primers were used as below:

Lys 389 Ala

Template: wildtypeAGT-pETM30

K389A Fp 5'- CAGGGCGCCATGGCCTCTCACAAGC -3'

K389A Rp 5'- GACCCGACGCGGTTACAGCGCCTT**CGC**GGGGCAGTGCTG -3'

The PCR reaction system for K389A mutagenesis was set up and proceeds as shown in Table.1.

Table.1 PCR reaction system for K389A mutagenesis

5 µl	10X Phusion buffer
5 µl	dNTP mix (2 mM each dATP, dCTP, dGTP, dTTP)
5 µl	5'-end primer (10 pmol/µl)
5 µl	3'-end primer (10 pmol/µl)
0.5 µl	Wildtype AGT gene in pETM-30 as template
1.0 µl	Phusion polymerase (2.5 U/l)
28.5µl	water

Cycle steps	Temperature (°C)	Time (sec)	Number of cycles
Initial denaturation	98	30	1
Denaturation	98	10	30
Annealing	56	30	30
Elongation	72	45	30

After PCR reaction, the product was purified from agarose gel after electrophoresis using NucleoSpin Extract II Kit and the concentration was measured by UV absorbance at 260nm with a nanodrop-spectrophotometer.

1.1.2 T4 treatment of PCR product

For the next step, 0.2 pmol of extracted PCR product was treated with T4 DNA polymerase in the presence of dATP to make complementary overhangs. The chemicals were mixed in a tube as Table.2.

Table.2 T4 polymerase treatment of PCR product

2 µl	10X New England Biolab Buffer 2
0.2pm	K389A PCR product
0.5 µl	dATP (100 mM)
1 µl	DTT (100 mM)
0.2 µl	100X BSA
0.4 µl	T4 DNA polymerase (3units/µl)

Sterile water was added to make total volume of 20 µl.

The mixed solution was spin for 1 min at 1.3k rpm in a microcentrifuge and incubated for 30 min at room temperature followed by 75 °C treatment for 20min to inactivate the polymerase. Then spin for 1min at 1.3k rpm.

1.1.3 Linearization of the expression vector (LIC vector) by *BsaI* digestion

The pETM-11/LIC and pETM-20/LIC vectors were transformed to *E.coli* DH5α using heat shock transformation, after which the amplified vectors were extracted from the cells by a miniprep kit (Qiagen) and the concentration was measured at 260nm wavelength.

The linearization of the LIC vectors was done with *BsaI* in 1.5ml eppendorf tubes. The digestion mix was incubated at 50 °C for 1h.

Table. 3 Linearization of LIC vector

5 μ l	10X New England Biolabs Buffer 3
5 μ g	pETM-11/LIC & pETM-20/LIC
2.5 μ l	<i>Bsa</i> I (10 unit/ μ l)

Sterile water was added to make total volume of 50 μ l

To minimize the amount of undigested vectors after *Bsa*I treatment, the bands with the correct size for the linear vector were cut out of the agarose gel after electrophoresis and extracted from it.

1.1.4 T4 DNA polymerase treatment of the linear LIC vector

About 600 ng of *Bsa*I-digested LIC vectors were treated with T4 DNA polymerase. The reaction system was set up as shown in Table.4.

Table.4 T4 DNA polymerase treatment of the linear LIC vector

2 μ l	10X New England Biolabs Buffer 2
600ng	<i>Bsa</i> I-digested pETM-11/LIC & pETM-20/LIC
0.5 μ l	dTTP (100 mM)
1 μ l	DTT (100 mM)
0.2 μ l	100X BSA
0.4 μ l	T4 DNA polymerase (3units/ μ l)

Sterile water was added to a volume of 20 μ l

Followed by 13000 rpm spin for 1 min, the reaction mixtures were incubated at room temperature for 30 min, and incubated at 75 °C for 20 min to inactivate the polymerase, which was removed by 13000rpm centrifuge.

1.1.5 Annealing of the insert and the LIC vector and transformation

1 μ l T4 DNA polymerase treated linear pETM-11/LIC or pETM-20/LIC vectors were mixed with 0.02 pmol T4 treated K389A gene, incubating for 5min at room temperature for annealing. The total annealing products were transformed into Solopack supercompetent cells (Invitrogen), incubating on ice for 30min, followed by 1min heat shock and 2min on ice again. The cells were cultured in LB medium at 37 °C for 1 hour, plated onto LB agar plate with Kanamycin and incubated overnight at 37 °C.

1.1.6 Identification of positive mutation

Cloning PCR was used for identifying the positive K389A gene constructs. Table.5

shows the reaction system. For each plate with colonies containing pETM-11/LIC and pETM-20/LIC vector, they were picked up randomly and added into the PCR reaction solution and simultaneously grew on an agar plate with Kanamycin. For the cloning PCR, three kinds of control were used as shown in Table.6 to Table.8. The three main steps for the PCR reaction (denaturation at 94 °C for 30s, annealing at 60 °C for 30s and extension at 68 °C for 210s) were repeated for 30 cycles.

Table.5 Cloning PCR reaction system

10 µl	Master mix (2x)
2 µl	T7 primer Forward
2 µl	K389A primer Reverse
6 µl	water
	One colony

Table.6 Control 1 for the cloning PCR

10 µl	Master mix (2x)
2 µl	T7 primer Forward
2 µl	K389A primer Reverse
5.5 µl	water
0.5 µl	template

Table.7 Control 2 for the cloning PCR

10 µl	Master mix (2x)
2 µl	T7 primer Forward
2 µl	T7 primer Reverse
5.5 µl	water
0.5 µl	template

Table.8 Control 3 for the cloning PCR

10 µl	Master mix (2x)
2 µl	T7 primer Forward
2 µl	T7 primer Reverse
6 µl	water
	One colony from pETM-11/ LIC plate

The positive transformants were identified in an agarose gel after electrophoresis. Two of them with pETM-11/LIC vector and the other two with pETM-20/LIC were selected and cultured in 3ml LB medium with Kanamycin.

Finally, the plasmids were extracted from the cells using a miniprep kit. The concentrations were measured by UV absorbance at 260nm and the DNA sequences were determined (Eurofins MWG GmbH).

1.2 Transformation

The pETM-20/LIC with AGT mutant gene insertion was selected as plasmid for expression (Fig.8)

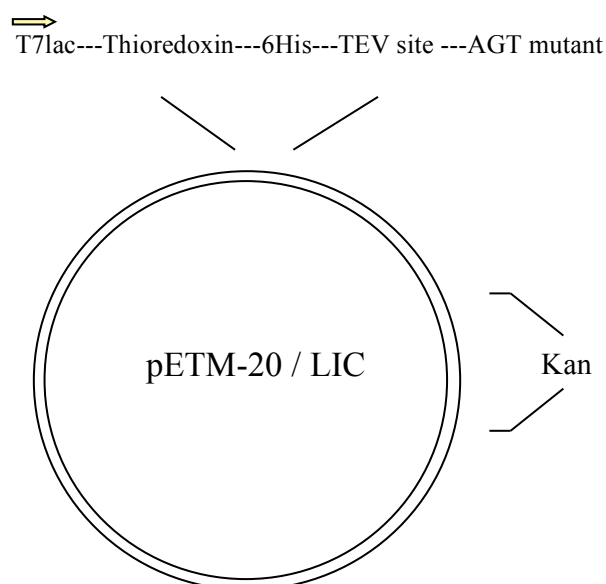


Fig.8 pETM-20/LIC vector

In order to transform the plasmids into the T7 polymerase expression *E.coli* BL21(DE3)-RIL competent cells, one tube of cells and 1 μ l plasmids were mixed and incubated on ice for 30 min, followed by 42°C water bath for 60s and on ice for 2 min. After addition of 250 μ l SOC broth, it was shaken for 1 h at 37°C. Then the cells were spread onto the LB plate with both Kanamycine and Chloramphenicol and incubated overnight at 37°C.

1.3 Protein Expression

The colonies growing up on LB plate were picked up and transferred to 10 ml LB medium with Kanamycine and Chloranphenicol for overnight pre-culture. For scaling up, 10 ml was pipeted into two 1 L TB containing Kanamycine and Chloramphenicol. When OD₆₀₀ value reached around 1.5 under 37°C incubation, 1 ml of 250 mM IPTG was added to the flasks and cultured overnight at 21°C.

1.4 Purification

1.4.1 Cell lyses

After centrifugating at 5500 rpm for 20 min and discarding the supernatant, the cell pellet were resuspended with bufferA (50mM HEPES pH7.5, 150mM NaCl, 50mM Imidazole, 2mM BME) followed by addition of some DNase, protease inhibitor and lysozyme. The cells were lysed by sonification to release proteins. After that, the cell debris was discarded by centrifugation at 19000 rpm for 60 min, and the lysate solution was filtered through a 45 µm filter.

1.4.2 Purification

Column chromatography on Nickel affinity matrices was used for first step purification. The sample was loaded after the column reached equilibrium by about five column volumes of bufferA. After moving the unbound contaminants, the fusion protein which attached to the Nickel column by His-tag was eluted using about two column volumes of bufferB (50mM HEPES pH7.5, 150mM NaCl, 500mM Imidazole, 2mM BME). The concentration of the fusion protein was determined by UV absorbance at 280nm.

TEV protease treatment was carried out by adding TEV protease into the protein solution (1 tube/50ml). Then the solution was put into a 8000 MWCO dialysis bag against 600 ml buffer A, incubating at 4°C overnight to separate the protein from His-tag.

The Nickel column was used for the second time for the TEV treated protein sample. The flow-through was collected since the His-tag attaches to the Ni-matrix. The sample was concentrated to 5 ml by centrifugation at 4000 rpm in a 8000 MWCO concentrator (Corning Spin-X UF).

Gel filtration in an FPLC system (GE Healthcare) using SephadexG-200 column was the next purification step. 5ml concentrated sample was injected and eluted by GF buffer (50mM HEPES pH7.5, 150mM NaCl, 2mM BME). The 96-well plate was used for collection and the flow rate was set to 1.0ml/min. According to the UV spectrum at 280nm detection and SDS-PAGE, the separated fractions were pooled together and stored at -80°C.

2. Pex5p (TPR domain) preparation

Pex5p C-terminus gene has been cloned in pETM-30 vector with GST tag. (Fig.9)

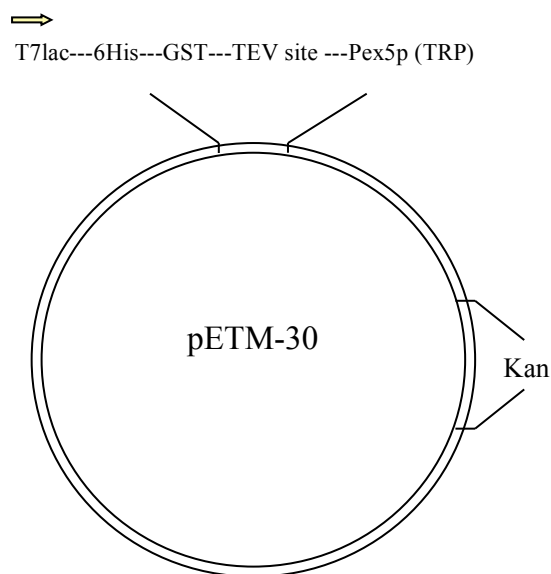


Fig. 9 The pETM-30 vector

The purification step of Pex5p was almost the same as AGTs, except that the size exclusive chromatography used was SephadexG-75. Besides, Pex5p-GST fusion protein for GST pull down experiment was prepared by Nickel column without further TEV treatment.

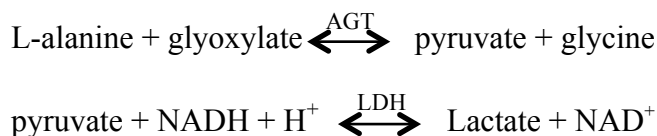
3. Glutathione S-Transferase (GST) pull down assay

Glutathione-sepharose beads are able to immobilize Pex5p-GST fusion protein. If binding to Pex5p, the AGT mutant would not be washed away from the beads until eluted by L-Glutathione (pH 8.0). Then its presence in elution can be detected using SDS-PAGE.

About 400µl glutathione-sepharose beads liquid was added into each eppendorf tubes, centrifuged for 2 min at 1.3k rpm and the supernatent was piped out. 600µl GF buffer was used to wash the beads, repeating for three times. 200µl Pex5p-GST fusion protein was added to the beads and incubated for 3 min followed by centrifuging for 2 min to remove the unbound substances. Then 0.6 mg of the six mutants, 0.2 mg sterol-carrier protein (SCP2, as the positive control) and 0.6 mg Pex19 (as the negative control) were respectively added to the beads which immobilized Pex5p-GST. After incubating for 10 min, the flow-through was removed and GF buffer was used to wash the beads for three times. Finally, 100µl of 20mM fresh prepared L-Glutathione (pH 8.0) was used for elution. The result was detected by SDS-PAGE.

4. Enzyme Activity Measurement

The pyruvate assay is a method to measure enzyme activity of human AGT with high sensitivity, which needs two step reactions as following:



The amount of produced pyruvate by AGT catalysis can be estimated through measuring the consumed NADH as a decrease in extinction at 340nm. Thereby the AGT activity can be calculated.

However, not only pyruvate but also glyoxylate is able to react with NADH in the presence of lactate dehydrogenase (LDH), which would affect the accuracy of AGT activity measurement. In order to eliminate glyoxylate effect, it is necessary to add Tris pH 8.2 to the products of the first reaction step. The idea is that glyoxylate forms a Schiff base with Tris so that it would not be the substrate of LDH any longer, but pyruvate oxidation of NADH is not affected (Thompson, 1968 and Rowsell *et al*, 1972).

The reaction was carried out with 2 μ g AGT in 100mM potassium phosphate pH 8.0, in the presence of 0.15mM pyridoxal-5'-phosphate (PLP), 10mM glyoxylate and 150mM alanine were used as substrates. The reaction was performed in a total volume of 300 μ l for about 30 minutes at 37°C. The same reaction was performed without the addition of AGT as the negative control. The reaction was stopped by adding 50 μ l of 50% TFA followed by 5 minutes centrifugation at high speed. Subsequently, 2 μ l of the reaction product was mixed with 250mM Tris pH 8.2 and waited for 5min until Tris-glyoxylate complex was completely formed. Then 0.25 mM NADH and 5 μ l LDH were added to make a total volume of 100 μ l. After about 10min, the measurement was carried out at 340 nm in a TECAN Infinite 1000 spectrophotometer.

Enzyme activities were also measured in the presence of 5 μ M Pex5p.

The formula for calculation is as following:

$$\text{Enzyme activity}(\mu\text{mol/h/mg}) = \frac{(\text{ABS}_{\text{Control1}} - \text{ABS}_{\text{mutant}}) \times 0.1\text{ml} \times 350\text{u1} \times 1000}{6220 \left(\text{ml} \times \text{mmol}^{-1} \times \text{cm}^{-1} \right) \times 0.294\text{cm} \times 2\text{u1} \times t(\text{h}) \times 0.002\text{mg}}$$

5. Circular dichroism (CD) measurement

Secondary structure content of a macromolecule can be determined by CD spectroscopy in the far-UV region (190nm-250nm). Alpha-helix, beta-sheet and random coil structures each give rise to a characteristic shape and magnitude of CD spectrum. Due to the sensitivity of secondary structure to its environment, CD is useful to observe how secondary structure changes with environmental conditions or on interaction with other molecules.

The AGT mutants and the wildtype protein were diluted to 0.2mg/ml, then dialyzed overnight in 10mM pH 8.0 phosphate buffer. The measurements were performed on a Jasco J-810 spectropolarimeter setting up to 1 nm bandwidth, 1 s response, 1 nm data pitch and 100 nm/min scan speed. UV spectra were recorded between 195nm and 260nm. First the buffer was run for three times as blank. Then CD values of each AGT mutant as well as wildtype were measured for three times.

6. Isothermal Titration Calorimetry (ITC) experiment

Isothermal Titration Calorimetry is a gold standard for measuring biomolecular interactions. ITC simultaneously determines all binding parameters in a single experiment, such as the stoichiometry of the interaction (n), the dissociation constant (K_d), enthalpy (ΔH) and entropy (ΔS), and heat capacity of binding (ΔC) and the free energy (ΔG) can be calculated from these directly measured parameters.

For this experiment, Pex5p acted as the ligand, which was concentrated to around 0.27 mM, approximately to a ten times higher concentration than the AGT mutants with about 0.027 mM. Before carrying out ITC experiment, the two samples were dialyzed together in a 8000 MWCO dialysis bag against GF buffer over night in the cold room, followed by centrifugation at 13000 rpm to remove possible precipitation. The measurement was performed at 25°C in the VP-ITC machine, where the AGT solution was titrated by Pex5p, using 10 μ l injection volumes, 240s incubation time between the injections and a stirring speed of 307 rpm. Origin 7.0 was used for data processing. The ITC measurement for each AGT mutants was repeated three times.

7. Crystallization of K390A-Pex5p & K390A/K391A-Pex5p complex

Pex5p (TPR) and K390A were mixed in a 3:2 molar ratio and concentrated to about 5mg/ml followed by 13000 rpm centrifugation for 5 min. In terms of the pre-known crystallization condition of the wildtype AGT- Pex5p complex as starting point (0.1M Bis-Tris pH 5.3, 0.15M LiSO₄, 17% PEG3350), a 24 well plate was set up as shown

in fig. 10 using the hanging drop vapor diffusion method at 20°C. Each well was filled with 500 µl reservoir solution. Then 1µl protein and 1µl reservoir solution was mixed in each cover slide to grow crystals. The same procedure was used for making the K390A/K391A-Pex5p (TPR) complex crystals.

Fig.10 Crystallization condition screening for AGT mutant-Pex5p complexes

0.1M Bis-Tris 0.1M LiSO ₄ 12% PEG 3350	0.1M Bis-Tris 0.1M LiSO ₄ 15% PEG 3350	0.1M Bis-Tris 0.1M LiSO ₄ 17% PEG 3350	0.1M Bis-Tris 0.1M LiSO ₄ 19% PEG 3350	0.1M Bis-Tris 0.1M LiSO ₄ 21% PEG 3350	0.1M Bis-Tris 0.1M LiSO ₄ 25% PEG 3350
0.1M Bis-Tris 0.15M LiSO ₄ 12% PEG 3350	0.1M Bis-Tris 0.15M LiSO ₄ 15% PEG 3350	0.1M Bis-Tris 0.15M LiSO ₄ 17% PEG 3350	0.1M Bis-Tris 0.15M LiSO ₄ 19% PEG 3350	0.1M Bis-Tris 0.15M LiSO ₄ 21% PEG 3350	0.1M Bis-Tris 0.15M LiSO ₄ 25% PEG 3350
0.1M Bis-Tris 0.17M LiSO ₄ 12% PEG 3350	0.1M Bis-Tris 0.17M LiSO ₄ 15% PEG 3350	0.1M Bis-Tris 0.17M LiSO ₄ 17% PEG 3350	0.1M Bis-Tris 0.17M LiSO ₄ 19% PEG 3350	0.1M Bis-Tris 0.17M LiSO ₄ 21% PEG 3350	0.1M Bis-Tris 0.17M LiSO ₄ 25% PEG 3350
0.1M Bis-Tris 0.2M LiSO ₄ 12% PEG 3350	0.1M Bis-Tris 0.2M LiSO ₄ 15% PEG 3350	0.1M Bis-Tris 0.2M LiSO ₄ 17% PEG 3350	0.1M Bis-Tris 0.2M LiSO ₄ 19% PEG 3350	0.1M Bis-Tris 0.2M LiSO ₄ 21% PEG 3350	0.1M Bis-Tris 0.2M LiSO ₄ 25% PEG 3350

8. Data collection and structure determination

Diffraction data was collected at a temperature of 100 K at the bending magnet beamline X13 (EMBL/DESY). Single crystals of the K390A-Pex5p (TPR) and K390A/K391A-Pex5p (TPR) mutants were harvested with a nylon loop, cryo protected in mother liquor with 30% v/v glycerol and then directly flash-frozen in the beam line cryo-stream.

Structure determination was done by Dr. Krisztian Fodor. Data were integrated with MOSFLM and scaled with Scala. Both structures were solved by molecular replacement with Phaser using the wildtype AGT-Pex5p (TPR) complex as a search model (PDB code: 3R9A).

Starting from MR phases, the structure was manually rebuilt in COOT and atomic positions, individual B-factors and TLS parameters were refined with REFMAC.

Results

1. K389A mutant construction

PCR result of the K389A mutagenesis was shown in Fig11. The concentration of the PCR product was measured as 82.9 ng/μl.

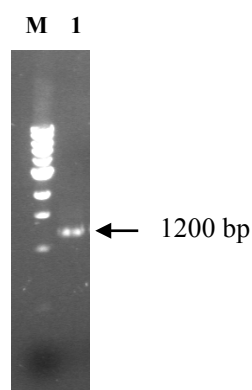


Fig.11 K389A gene amplification by PCR.
1- K390A DNA (~1200bp).

After ligase independent cloning and plasmids transformation to supercompetent cells, eight pETM-11/LIC transformants and five pETM-20/LIC transformants were picked up from the agar plates to perform the cloning PCR for evaluation. The result was shown in Fig 12. Four colonies which showed the bands pointed by the arrows were selected and cultured in 3 ml LB medium with Kanamycin, and the containing plasmids were extracted by miniprep kit and then sent out for DNA sequencing. The concentrations of these plasmids were 66.4 ng/μl, 56.4 ng/μl, 54.5 ng/μl and 49.0 ng/μl respectively.

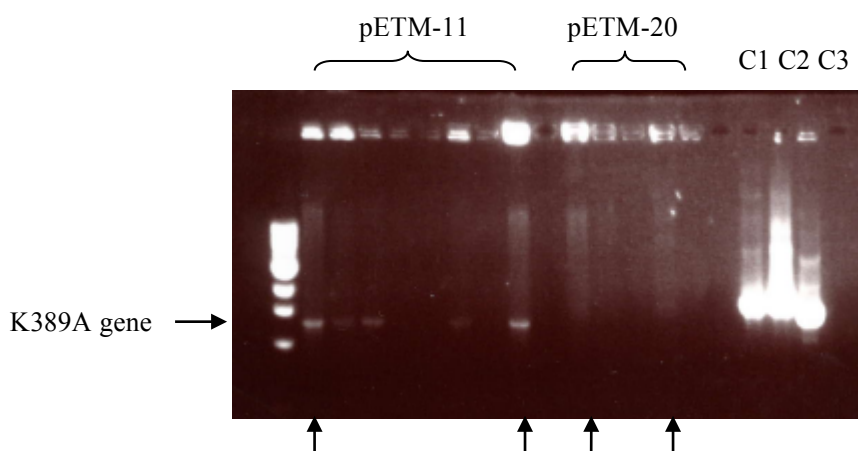


Fig 12. Cloning PCR of K389A. The pointed colonies were selected for DNA sequencing.

Comparing the DNA sequence of these test mutants to wildtype AGT (Fig.13), it indicated that the mutagenesis successfully changed residue-389 Lys to Ala as we expected. One of the pETM-20/LIC clones was selected for protein expression.

```

Length=392
Score = 805 bits (2079), Expect = 0.0, Method: Compositional matrix adjust.
Identities = 391/392 (99%), Positives = 391/392 (99%), Gaps = 0/392 (0%)

Query 1 MASHKLLVTPPKALLKPLSIPNQLLLGPGPSNLPPRIMAAGGLQMGSMKDMYQIMDEI 60
Sbjct 1 MASHKLLVTPPKALLKPLSIPNQLLLGPGPSNLPPRIMAAGGLQMGSMKDMYQIMDEI 60

Query 61 KEGIYVVFQTRNPLTLVISGSHCALEAALVNVLEPGDSFLVGANGIWGQRAVDIGERIC 120
Sbjct 61 KEGIYVVFQTRNPLTLVISGSHCALEAALVNVLEPGDSFLVGANGIWGQRAVDIGERIC 120

Query 121 ARVHPMTKDPGCHYTLQEVEEGLAQHKPVLLFLTHGESSTGVLPDGFELCHRYKCLL 180
Sbjct 121 ARVHPMTKDPGCHYTLQEVEEGLAQHKPVLLFLTHGESSTGVLPDGFELCHRYKCLL 180

Query 181 LVDSVASLGGTPLYMDRQCIDILYSGSQKALNAPPCTSLISFSDKAKKKMYSRKTKPFSF 240
Sbjct 181 LVDSVASLGGTPLYMDRQCIDILYSGSQKALNAPPCTSLISFSDKAKKKMYSRKTKPFSF 240

Query 241 YLDIKWLANFWGCDDQPRMYHHTIPVISLYSLRESLALIAEQGLENSWRQHREAAAYLHG 300
Sbjct 241 YLDIKWLANFWGCDDQPRMYHHTIPVISLYSLRESLALIAEQGLENSWRQHREAAAYLHG 300

Query 301 RLQALGLQLFVKDPALRLPTVTTVAVPAGYDWRDIVSYVIDHFDIEIMGGLGPSTGKVL 360
Sbjct 301 RLQALGLQLFVKDPALRLPTVTTVAVPAGYDWRDIVSYVIDHFDIEIMGGLGPSTGKVL 360

Query 361 IGLLGCNATRENVDRVTEALRAALQHCP KKL 392
Sbjct 361 IGLLGCNATRENVDRVTEALRAALQHCP A KKL 392

```

Fig.13 K389A DNA sequence aligned to wildtype AGT.

2. Purification of AGT mutants

The purified six AGT mutants were obtained after two-step Nickel affinity chromatography and gel filtration with Sephadex G-200 using FPLC. The separated fractions were pooled together, and loaded onto SDS-PAGE gel. Fig.14 and Fig.15 demonstrate typical examples of the gel filtration chromatogram and the SDS-PAGE gel for certain AGT mutants.

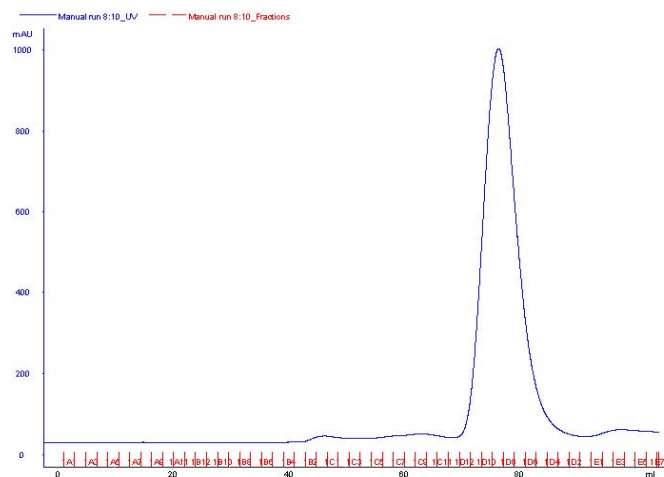


Fig.14 Gel filtration chromatogram of K390A at UV280nm

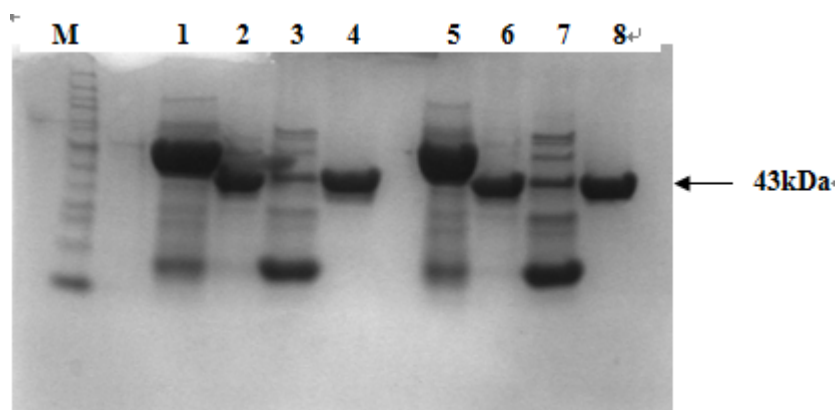


Fig.15 SDS-PAGE of K390A and K391A. 1- Ni first time of K390A; 2- Ni second time flowthrough of K390A; 3- Ni second time elution of K390A; 4- Gel filtration elution of K390A; 5- Ni first time of K391A; 6- Ni second time flowthrough of K391A; 7- Ni second time elution of K391A; 8- Gel filtration elution of K391A

Using pETM-20/LIC vector, BL21-RIL strain and TB culture medium for AGT mutants expression, a high yield was obtained.

The yield of AGT mutants was: $y = m / V$

Q385A	P388A	K389A	K390A	K391A	K390A/K391A
10.03 mg/L	12.40 mg/L	12.65 mg/L	10.55 mg/L	10.05 mg/L	14.06 mg/L

The same purification approach was used for Pex5p (TPR). The recorded UV spectrum of gel filtration by Sephadex G-75 column and SDS-PAGE gel were demonstrated in Fig.16 and Fig.17.

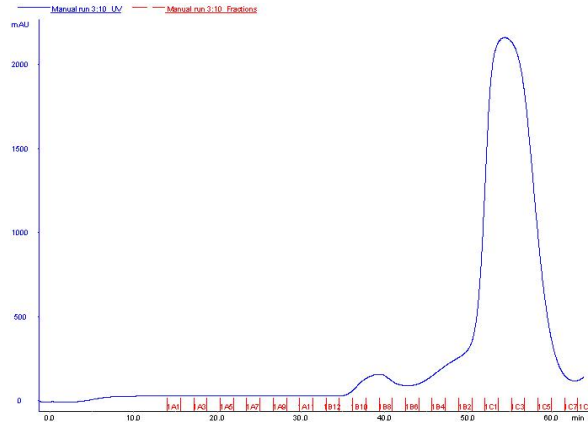


Fig. 16 Gel filtration chromatogram of Pex5p at UV280nm

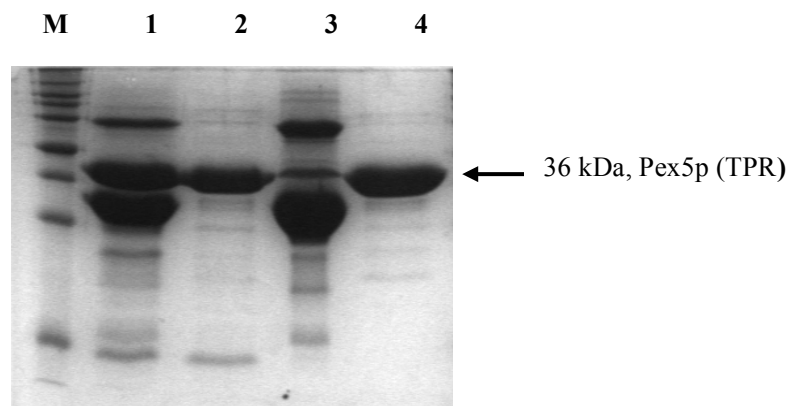


Fig.17 SDS-PAGE of Pex5p (TPR). 1- Ni first time elution; 2- Ni second time flowthrough; 3- Ni second time elution; 4- Gel filtration elution.

3. GST pull down

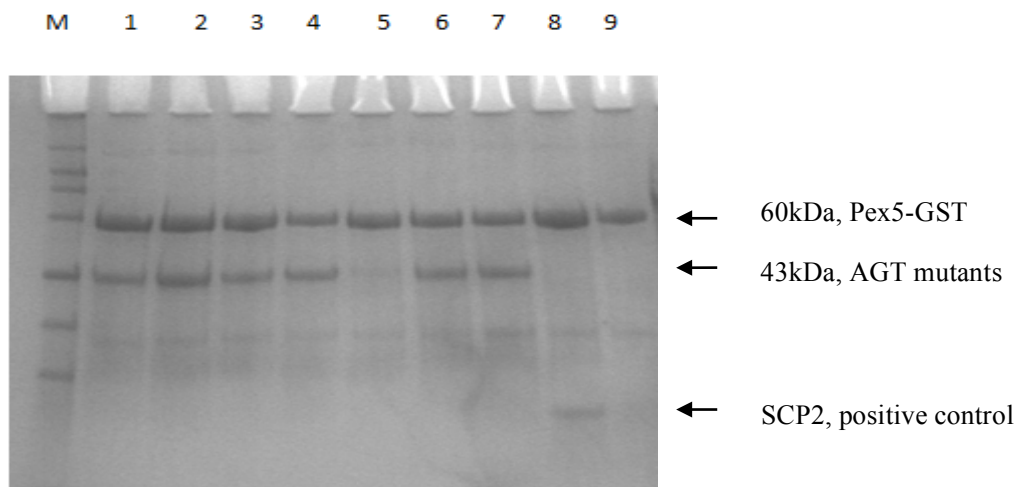


Fig.18. GST-pull down assay of AGT mutants with GST-Pex5p. 1-Q385A; 2- P388A; 3- K389A; 4- K390A; 5- K391A; 6- K390A/K391A; 7- wildtype AGT; 8- positive control (SCP2); 9- negative control (Pex19p).

According to the SDS-PAGE gel (Fig.18), it appeared that K391A did not bind to Pex5.

4. Enzyme activity measurement

For the enzyme reaction system without adding Pex5p, the reaction time was 30min. The absorbance of NADH was measured at 340nm by TECAN Infinite 1000 spectrophotometer as shown in Table.9.

Table.9 Absorbance of NADH at 340 nm (without Pex5p)

	Q385A	P388A	K389A	K390A	K391A	K390A/K391A	wtAGT	Control	blank
1	0.2485	0.3045	0.2748	0.2730	0.2837	0.2909	0.2891	0.3821	0.3818
2	0.2831	0.2709	0.3279	0.2942	0.2795	0.3009	0.3026	0.4155	0.3747
3	0.3436	0.2576	0.2808	0.2619	0.2533	0.2975	0.2375	0.4068	0.3906

The enzyme activities of wildtype AGT and mutants were calculated as described in the section of materials and methods.

The result was demonstrated in Table.10.

Table.10 Enzyme activities of AGT mutants and wildtype

	Q385A	P388A	K389A	K390A	K391A	K390A/K391A	wtAGT
1	1408.34	872.44	1156.66	1173.88	1071.49	1002.59	1019.81
2	1077.23	1193.98	-	971.00	1111.68	906.89	890.624
3	-	1321.26	1099.24	1280.11	1362.41	939.42	-
AV	1242.79	1129.23	1127.95	1141.67	1181.86	949.63	955.22

(Some bad data were abandoned.)

For the enzyme reaction system with addition of 5 μ M Pex5p, the reaction time was 35 min. The measured absorbance of NADH at 340 nm was shown in Table.11.

Table.11 Absorbance of NADH at 340 nm (with Pex5p addition)

	Q385A	P388A	K389A	K390A	K391A	K390A/K391A	wtAGT	Control	blank
1	0.2282	0.2259	0.2473	0.228	0.226	0.2639	0.2822	0.3868	0.3818
2	0.2413	0.2248	0.2526	0.2481	0.2621	0.2055	0.2677	0.4074	0.3747
3	0.2431	0.2139	0.2496	0.2338	0.2509	0.2713	0.2536	0.3982	0.3906

Table.12 reveals the calculated enzyme activity of AGT mutants and wildtype after

binding to Pex5p.

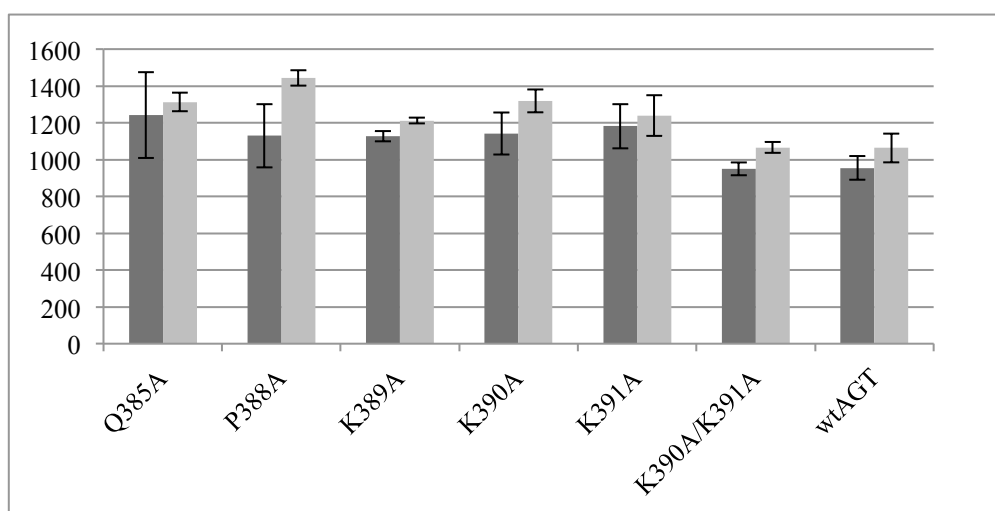
Table.12 Enzyme activities of AGT mutants and wildtype with Pex5p addition

	Q385A	P388A	K389A	K390A	K391A	K390A/K391A	wtAGT
1	1389.22	1408.10	1232.46	1390.86	1407.28	1096.22	946.031
2	1281.71	1417.13	1188.96	1225.90	1110.99	-	1065.03
3	1266.93	1506.59	1213.59	1343.26	1202.92	1035.49	1180.76
AV	1312.62	1443.94	1211.67	1320.01	1240.40	1065.85	1063.94

According to the NADH absorbance measured by TECAN Infinite 1000, it was noticed that the values of the control (without AGT, thereby no pyruvate production) and blank were almost the same. It means that the reaction of glyoxylate and NADH was totally inhibited by Tris, otherwise we would see the consumption of NADH which generates different values between control and blank.

As a result, the comparison of AGT activities between mutants, as well as the mutants and its Pex5p-binding complexes was demonstrated in Fig.19.

Fig.19 Comparison of AGT activities



A dramatic decrease could not be observed for the enzyme activities between the mutants and the wildtype with/without Pex5p, meaning that the AGT is almost fully active when binds to Pex5p.

5. CD measurement

CD data of the six AGT mutants and wildtype were recorded. The CD spectrum (Fig.20) was generated by the average values from three single measurements of each sample.

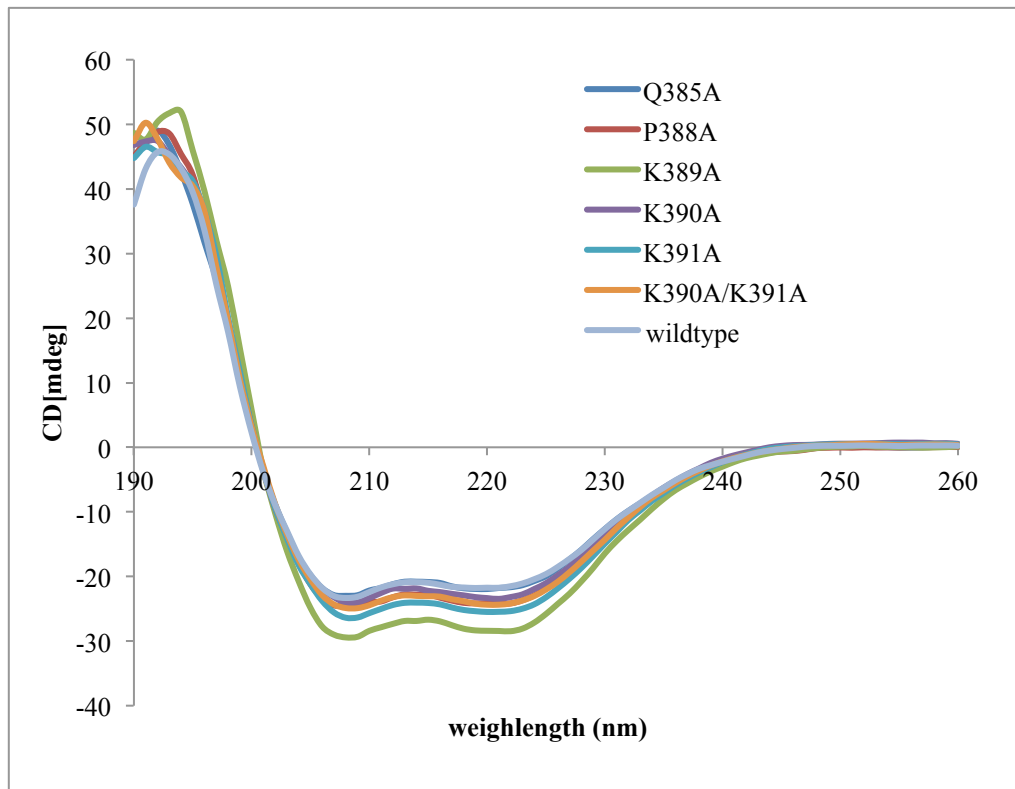
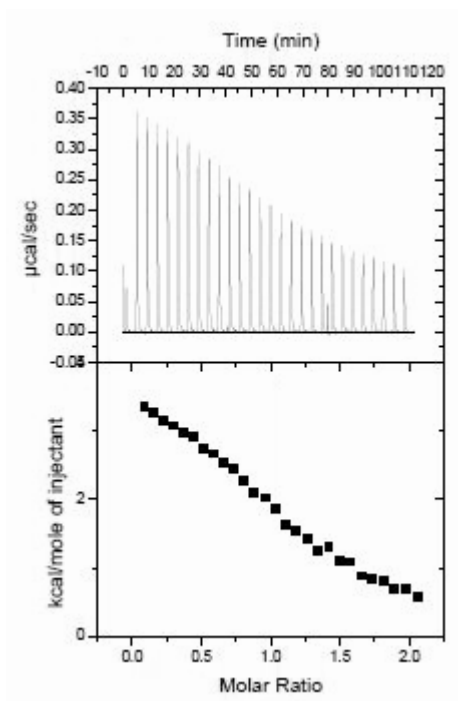


Fig.20 CD spectrum of AGT mutants and the wildtype.

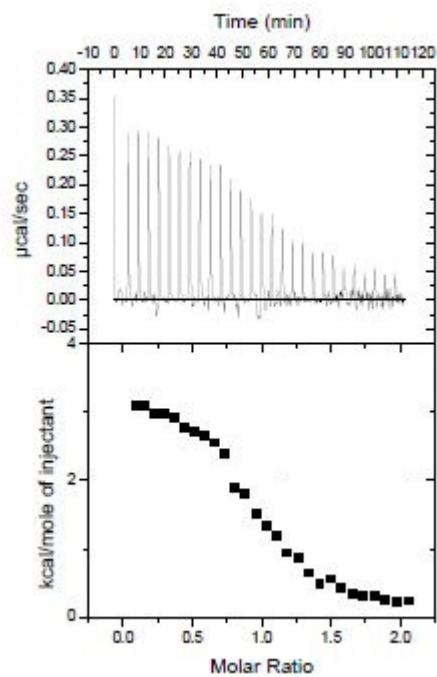
The two negative peaks at about 220nm and 208nm and the positive one at 190 nm indicated that the AGTs were primarily composed of α -helix as secondary elements, and there was no major conformation change among the wildtype AGT and mutants.

6. ITC experiment

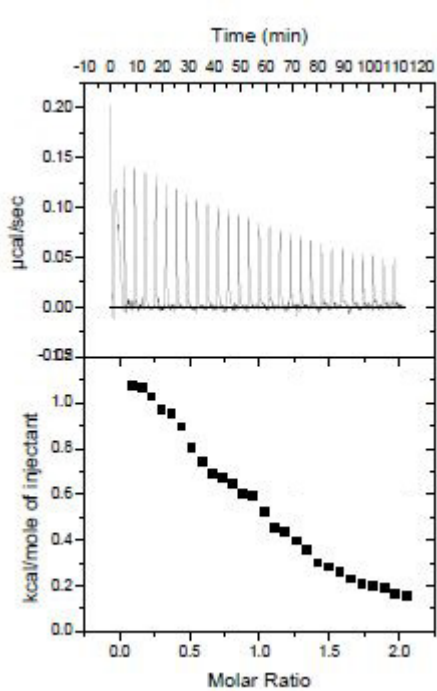
The values of K_a , ΔH and ΔS were measured directly from ITC experiment and generated using Origin 7. (Appendix II). The dissociation constant K_d was calculated by fomular: $K_d=1/K_a$. The typical spectra for each mutant were shown in Fig.21.



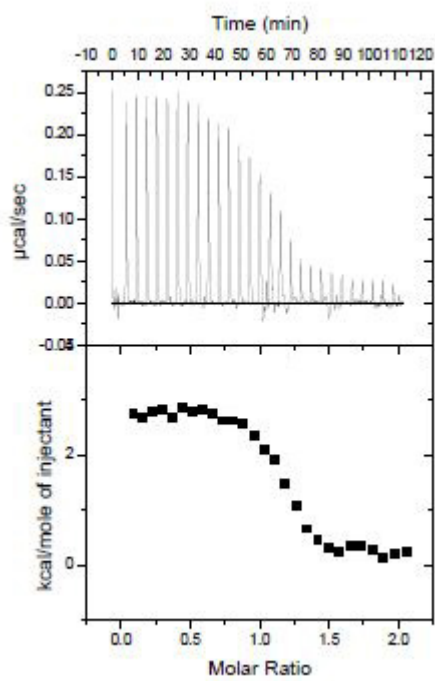
(a)



(b)



(c)



(d)

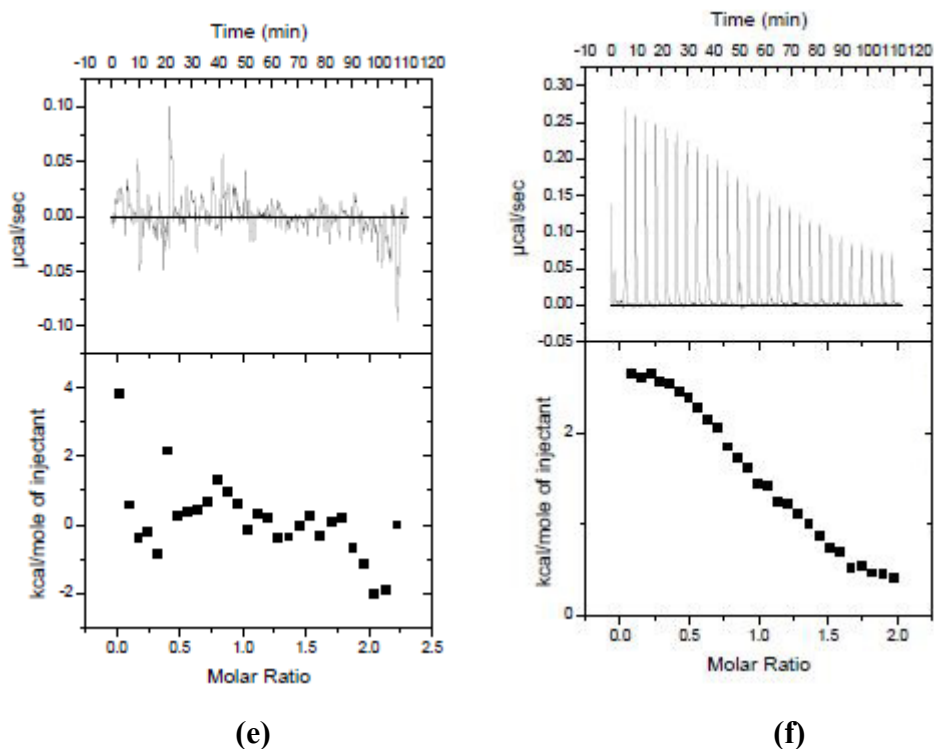
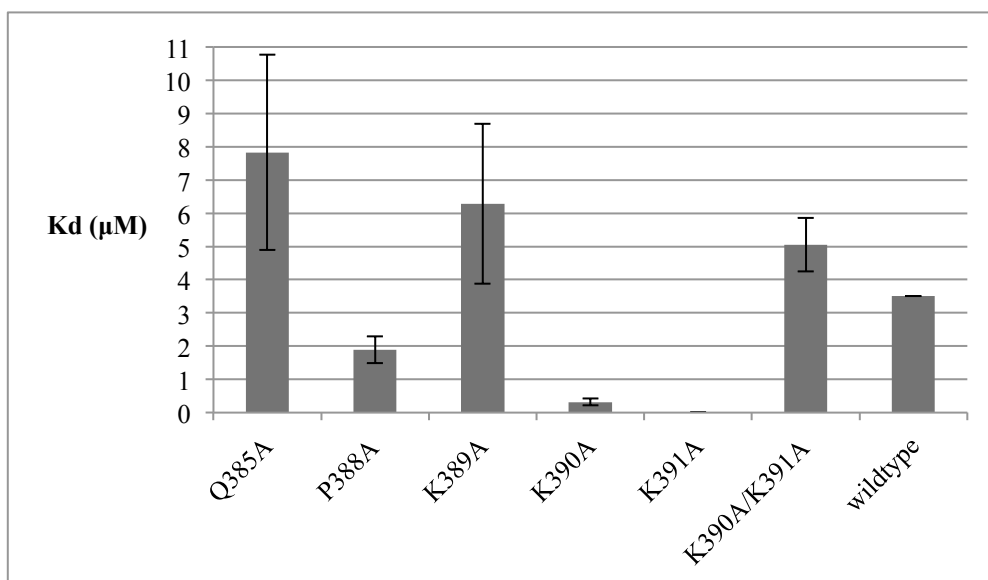


Fig.21 Typical ITC spectra of AGT mutants. (a) Q385A; (b) P388A; (c) K389A; (d) K390A; (e) K391A; (f) K390A/K391A.

As shown in Fig.21, K391A did not interact with Pex5p, which was also indicated by the GST-pull down. Not surprisingly, the binding affinity of Q385A and K389A became weaker than wildtype AGT ($K_d=3.5 \mu\text{M}$, measured by Fodor.K, unpublished) due to the interruption of hydrogen bonds between these mutated residues and Pex5p (shown in Fig.7(b) in the introduction part).

Fig.22 Dissociation constant (K_d) of the six mutants and wildtype AGT



However, it was unpredicted that lysine at 390 position of wildtype AGT, which does not seem to interact directly with Pex5p from structure view, demonstrated a dramatically increased binding affinity (about 10 times) when it was mutated to alanine. The lower binding affinity of K390A/K391A double mutant is also hard to explain, since the single mutant K390A shows a strong binding whereas K391A does not bind to Pex5p.

7. Crystallization of K390A-Pex5p (TPR) & K390A/K391A-Pex5p (TPR) complex, data collection and structure determination

The AGT-Pex5p (TPR) complex crystals were growing using hanging drop vapor diffusion method in 24-well plates at 20 °C for about three days. Among the test conditions, the most suitable one for K390A-Pex5p (TPR) complex was 0.1M Bis-Tris (pH 5.3), 0.1M LiSO₄ and 12% PEG 3350, and for K390A/K391A-Pex5p (TPR) was 0.1M Bis-Tris (pH 5.3), 0.17M LiSO₄ and 19% PEG 3350.

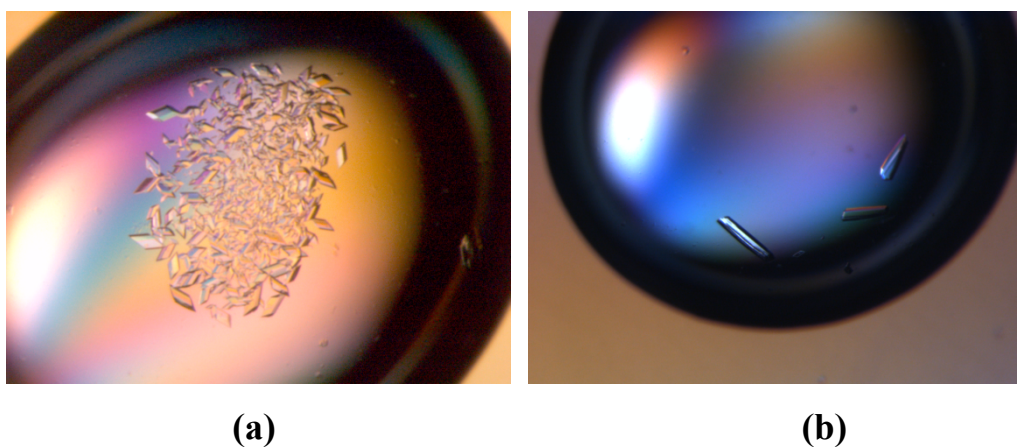


Fig.23 Crystal images of K390A and K390A/K391A double mutant. (a) K390A; (b) K390A/K391A.

Diffraction data was collected at the bending magnet beamline X13 in EMBL/DESY in Hamburg, Germany. After data processing, molecular replacement and structure refinement, the 3D-structure of K390A-Pex5p (TPR) complex was determined as shown in Fig.24. Data collection & refinement statistics are in Table.13. The complex of K390A/K391A-Pex5p have not solved yet. It was found that K390A was in form of dimer as the wildtype.

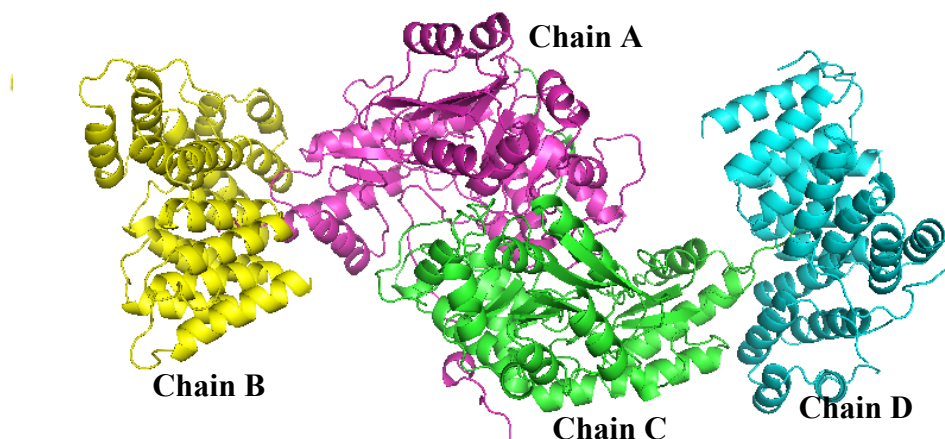


Fig.24 Structure of K390A-Pex5p (TPR) complex. Chain A,C-AGT dimer; Chain B,D-Pex5p TPR

Table.13 Data collection & refinement statistics

Beamline	X13, EMBL/DESY
Wavelength	0.81 Å
Detector	MARCCD 165 mm
Resolution (Å)	51.029-2.20 (2.32-2.20)
Space group	P 1
Cell parameters	$\alpha=57.66$ $\beta=74.79$ $\gamma=91.24$ a = 87.51 b = 83.69 c = 89.64
Number of observed reflections	190673
Number of unique reflections	73170
Completeness (%)	95.2(90.9)
Mosaicity (°)	0.93
I/ σ *	8.7 (2.0)
R _{sym} (%)	11.4 (46.6)
R _{work} (%)	17.7
R _{free} (%)	22.3
R.m.s. bond length (Å)	0.011
R.m.s. bond angles (°)	1.263
Number of residues	1371
Number of water molecules	731

The structural alignment of the mutant complex to the wild type is demonstrated in Fig.25 as an overview and Fig.26 shows a detailed picture of the PTS1 binding site.

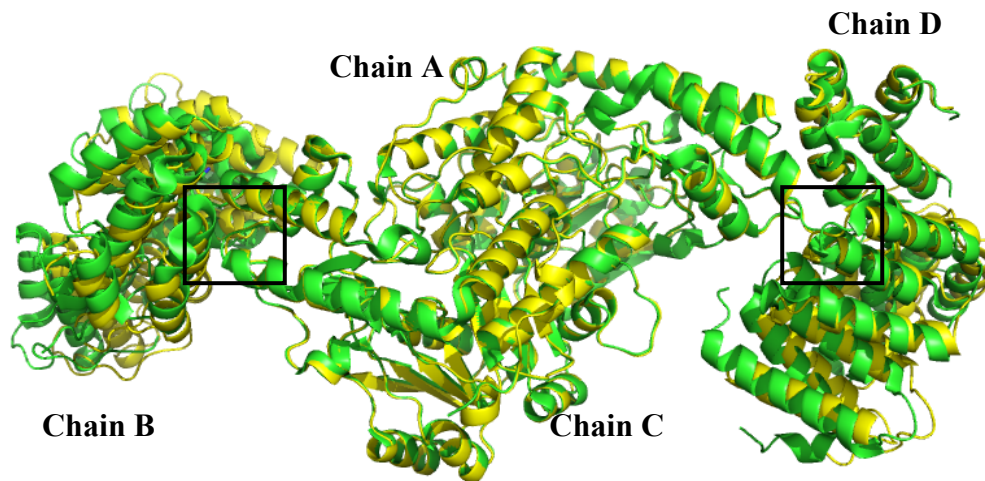


Fig.25 Alignment of K390A-Pex5p complex to the wildtype-Pex5p complex . The molecule in green is the mutant, and the one in yellow is the wildtype. The marked regions are the binding sites. The AGT molecule is complete identical, whereas a shift of Pex5p TPR domain in space can be seen obviously.

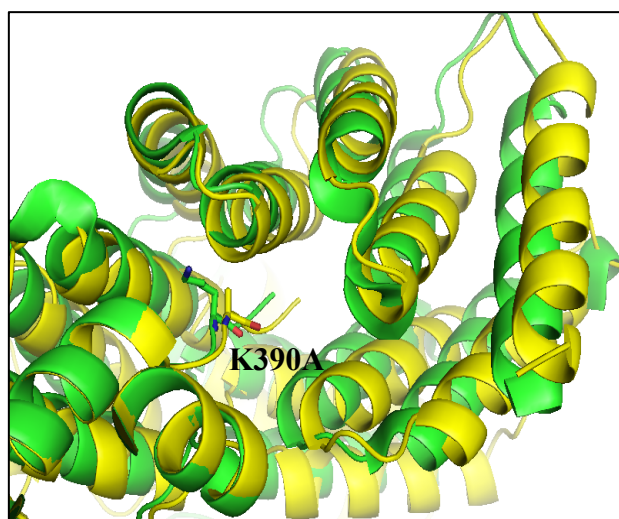


Fig.26 Binding site of Pex5p and K390A

We noticed that when compared to the wildtype protein, the position of the Pex5p TPR domain shifted a little in space when it interacted with K390A mutant. Some hints were obtained from the interface, which was calculated with PDBePISA (Table 14). It predicted that more hydrogen bonds and salt bridges were formed between

Pex5p (TPR) and K390A mutant, accompanied by the increased free energy, although the interface area appeared to be smaller.

Table.14 Interface between K390A and Pex5p (TPR)

	Interface area, Å ²	ΔG, kcal/mol	N _{HB}	N _{SB}
K390A & Pex5p (Chain A&B)	958.4	- 7.4	15	1
Wildtype & Pex5p (Chain A&B)	962.3	- 4.6	16	0
	Interface area, Å ²	ΔG, kcal/mol	N _{HB}	N _{SB}
K390A & Pex5p (Chain C&D)	990.1	- 6.6	19	2
Wildtype & Pex5p (Chain C&D)	1066.9	- 5.4	16	1

Discussion

Cloning, overexpression and protein purification protocols for human AGT mutants were established. It turned out that the vector pETM-20/LIC with Trx tag contributed to such high AGT production, compared to the protein yield in the previous studies of our lab (unpublished data) using pETM-30 with GST tag was much lower. Then the pETM-20/LIC was selected as the expression vector for this project.

The active human AGT forms a homodimer with a PLP molecule as cofactor for catalysis. There was no significant variation of enzyme activities between the AGT mutants with and without Pex5p addition, meaning that the mutation did not affect the catalytic site of the enzyme, even when bound to Pex5p.

For all mammals whose AGT gene has been sequenced, the PTS1s always have a two out of three match with the various consensus possibilities, which makes KKL of human AGT a unique one. There are several evidences suggesting that this special PTS1 is not as efficient as the consensus PTS1 in directing the peroxisomal import of AGT, e.g AGT-KKL did not compete with the import of endogenous catalase, whereas AGT-SKL did. The present project is the first time that full length human AGT variants with different PTS1 sequences rather than synthetic peptides from C-terminus have been used to study receptor-cargo interaction. Data from ITC experiment reveal that the non-consensus PTS1 of human AGT (-KKL) binds to Pex5p with very low affinity (lower μM range). Deeper understanding was obtained from both GST-pull down and ITC experiments of six residues mutations to alanine within or immediate upstream of tripeptide region. First, we found that the binding ability of human AGT to Pex5p depends on the lysine at -2 position (Lys 391) to large extent, revealed by the phenomenon that K391A did not interact with Pex5p in GST-pull down and ITC. However, it is particularly interesting that the lysine at -3 position (Lys 390) contributes to the low binding affinity of human AGT. It was observed from ITC experiment that the binding affinity increased by 10 times when this lysine mutated to alanine. Moreover, the double mutant of K390A/K391A showed a binding affinity that was only a little weaker than wildtype. These results suggest that it is the Lys 390 which determines the weak AGT-Pex5p interaction compared with other matrix proteins with consensus PTS1.

Comparing the structure of wildtype complex with K390A-Pex5p complex, we saw the shift of Pex5p TPR domain in space (Fig.25 and Fig.26). However, when aligning the mutant complex to another peroxisome matrix protein SCP2 (sterol carrier protein 2)-Pex5p complex, which has a consensus PTS1 as AKL, we found that the position of Pex5p TPR domains of these two different complexes almost overlaps (Fig.27). As a consequence, AGT-AKL mutant and SCP2 (-AKL) interact with the same Pex5p

(TPR) conformation.

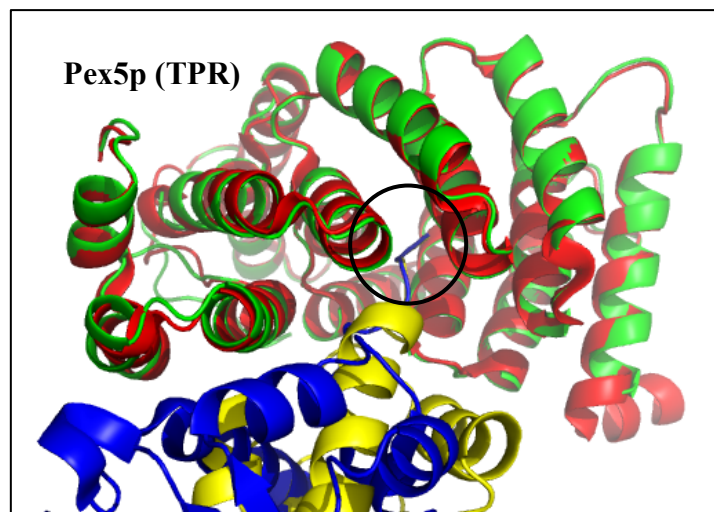


Fig.27 Alignment of AGT K390A-Pex5p complex to SCP2-Pex5p complex. The chains in green and red are from Pex5p, and the yellow chains are from AGT, blue ones are from SCP2. The PTS1 (-AKL) binding site is highlighted.

Fig.28 (a) shows the structure of unloaded Pex5p C-terminus domain, and Fig.28 (b) shows the comparison of its conformation changes upon binding to wildtype AGT-KKL and SCP2-AKL. According to previous studies (Stanley, 2006), the C-terminus of Pex5p switches from an open, snail-like conformation into a closed, circular conformation and these changes are caused by a long loop C terminal to the 7-fold tetratricopeptide repeat segments. According to the result of our project, the Pex5p TPR domain is flexible enough to adapt to various cargoes with different PTS1 sequence.

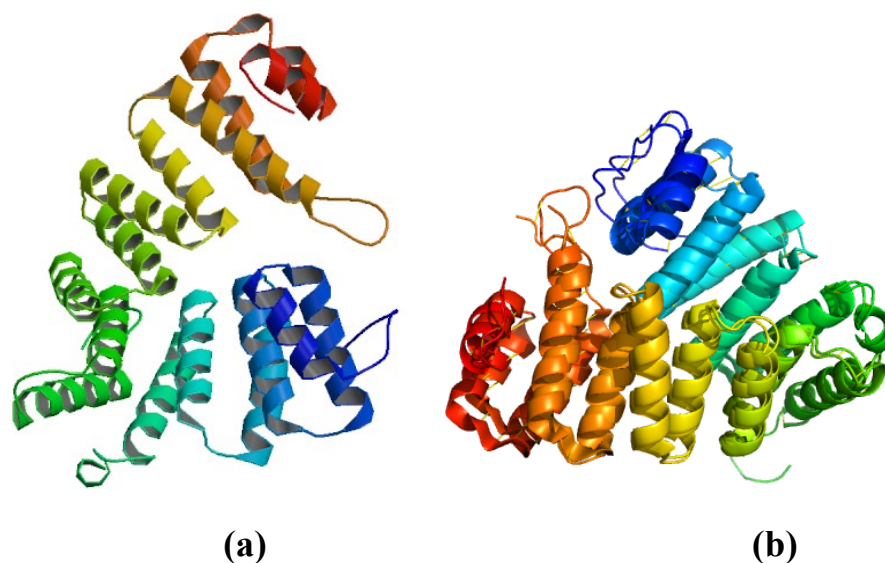


Fig.28 Conformation of unloaded Pex5p C-terminus and loaded with SPC2 and human AGT. (a) unloaded C-terminus of Pex5p (b) alignment of Pex5p C-terminus when binding to SPC2 and human AGT respectively.

Reference

Brocard C., Hartig A., Peroxisome targeting signal 1: Is it really a simple tripeptide?, *Biochimica et Biophysica Acta*. 1763 (2006), pp. 1565-1573.

Brocard C., Kragler F., Simon M.M., Schuster T., Hartig A. The tetratricopeptide repeat-domain of the PAS10 protein of *Saccharomyces cerevisiae* is essential for binding the peroxisomal targeting signal-SKL. *Biochem. Biophys. Res. Commun.* 204 (1994), pp. 1016-1022.

Danpure C., Primary hyperoxaluria type 1 and peroxisome-to-mitochondrion mistargeting of alanine:glyoxylate aminotransferase. *Biochimie (Paris)*. 75 (1993), pp. 309-315.

Erdmann R. and Schliebs W., Peroxisomal matrix protein import: the transient pore model, *Nat. Rev. Mol. Cell Biol.* 6 (2005), pp. 738–742.

Gouveia A.M., Reguenga C., Oliveira M., Miranda C. and Azevedo J., Characterization of peroxisomal Pex5p from rat liver. Pex5p in the Pex5p–Pex14p membrane complex is a transmembrane protein, *J. Biol. Chem.* 275 (2000), pp. 32444–32451.

Gould S.J., Keller G.A., Hosken N., Wilkinson J. and Subramani S., A conserved tripeptide sorts proteins to peroxisomes, *J. Cell Biol.* 108 (1989), pp. 1657–1664.

Ghosh D., Jeremy M., Berg A., Proteome-wide perspective on Peroxisome Targeting Signal 1(PTS1)-Pex5p affinities, *J. AM. Chem SOC.* 132 (2010), pp. 3973–3979.

Holroyd C. and Erdmann R., Protein translocation machineries of peroxisomes, *FEBS Lett.* 501 (2001), pp. 6–10.

Hettema E., Distel B. and Tabak H., Import of proteins into peroxisomes, *Molecular Cell Research*, 1451 (1999), pp.17-34.

Huber P.A., Birdsey G.M., Lumb M.J., Prowse D.T., Perkins T.J., Knight D.R. and Danpure C.J., Peroxisomal import of human alanine:glyoxylate aminotransferase requires ancillary targeting information remote from its C terminus, *J.Biol.Chem.* 280 (2005), pp. 27111–27120.

Klei.I.J.van der and Veenhuis.M, PTS1-independent sorting of peroxisomal matrix

proteins by Pex5p, *Molecular Cell Research*, 1763 (2006), pp. 1794-1800.

Kiel J.A.K.W., Emmrich K., Meyer H.E. and Kunau W.H., Ubiquitination of the peroxisomal targeting signal type 1 receptor, Pex5p, suggests the presence of a quality control mechanism during peroxisomal matrix protein import, *J. Biol. Chem.* 280 (2005), pp. 1921–1930.

Lametschwandtner G., Brocard C., Fransen M., Berger J. and Hartig A., The difference in recognition of terminal tripeptides as peroxisomal targeting signal 1 between yeast and human is due to different affinities of their receptor Pex5p to the cognate signal and to residues adjacent to it. *J.Biol.Chem.* 273 (1998), pp. 33635–33643.

Lazarow P.B. and Fujiki Y., Biogenesis of peroxisomes, *Annu. Rev. Cell Biol.* 1 (1985), pp. 489–530.

Motley A., Lumb M.J., Oatey B., Jennings P.R., Priyal A., Wanders R.J.A., Henk F., Danpure J., Mammalian alanine/glyoxylate aminotransferase 1 is imported into peroxisomes via the pts1 translocation pathway. increased degeneracy and context specificity of the mammalian pts1 motif and implications for the peroxisome-to-mitochondrion mistargeting of AGT in Primary Hyperoxaluria Type 1, *The Journal of Cell Biology*, 131 (1995), pp. 95-109.

Neuberger G., Maurer S.S., Eisenhaber B., Hartig A. and Eisenhaber F., Prediction of Peroxisomal Targeting Signal 1 Containing Proteins from Amino Acid Sequence, *Journal of Molecular Biology*, 328 (2003), pp.581-592.

Platta H.W., Girzalsky W. and Erdmann R., Ubiquitination of the peroxisomal import receptor Pex5p, *J. Biol. chem.* 384 (2004), pp. 37–45.

Purdue P.E. and Lazarow P.B., Peroxisome biogenesis, *Annu. Rev. Cell Dev. Biol.* 17 (2001), pp. 701–752.

Rowsell E.V., Carnie J.A., Snel K. and Taktak B., Assays for glyoxylate aminotransferase activities, *J.Biochem*, 3 (1972), pp. 247-257.

Stanley W.A, Fodor K., Schliebs W. and Wilmanns M., Protein translocation into peroxisomes by ring-shaped import receptors, *FEBS Letters*, 581 (2007), pp 4795–4802.

Stanley W.A., Filipp F.V., Kursula P., Schuller N., Erdmann R., Schliebs W., Sattler M. and Wilmanns M., Recognition of a functional peroxisome type 1 target by the dynamic import receptor Pex5p, *Mol. Cell*, 24 (2006), pp. 653–663.

Swinkels B.W., Gould S.J. and Subramani S., Targeting efficiencies of various permutations of the consensus C-terminal tripeptide peroxisomal targeting signal, *FEBS Lett.* 305 (1992), pp. 133–136.

Thompson J.S., Richardson K.E., Determination of pyruvate in enzyme-catalyzed reactions in the presence of glyoxylate, *Analytical Biochemistry*, 24 (1968), pp. 197-201.

Veenhuis M. and van der Klei I.J., Peroxisomes: flexible and dynamic organelles, *Current Opinion in Cell Biology*. 14 (2002), pp. 500-505.

Wang D.Y., Visser N.V., Veenhuis M. and van der Klei I.J., Physical interactions of the peroxisomal targeting signal 1 receptor Pex5p, studied by fluorescence correlation spectroscopy, *J. Biol. Chem.* 278 (2003), pp. 43340–43345.

Wanders R.J.A., Ruiter J., Schutgens R., Ofman R., Jurriaans S. and Tager J.M., Human liver L-alanine – glyoxylate aminotransferase: characteristics and activity in controls and hyperoxaluria type I patients using a simple spectrophotometric method, *Clinica Chimica Acta*, 189 (1990), pp.139-144.

Williams C., Stanley A., Peroxin 5: A cycling receptor for protein translocation into peroxisomes, *The International Journal of Biochemistry & Cell Biology*, 42 (2010), pp.1771–1774.

Part B

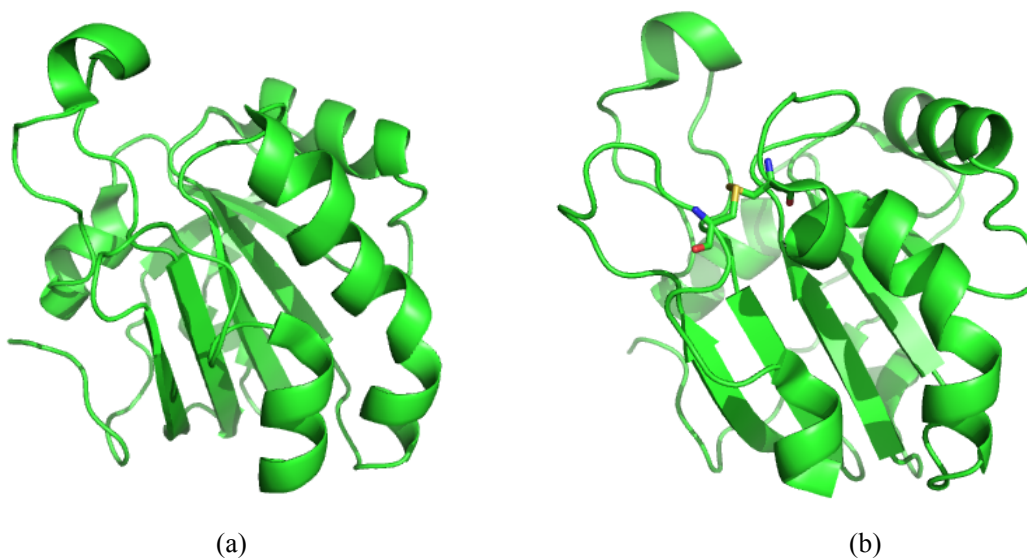
Human Peroxiredoxin 5

Introduction

1. PRDX5 and its structure

Peroxiredoxins (PRDXs) are a ubiquitous family of antioxidant enzymes, which control the levels of reactive oxygen species in cells and tissues and protect them against oxidation (Rhee *et al*, 2001 and Hofmann *et al*, 2002). PRDXs are able to reduce hydrogen peroxide, alkyl hydroperoxides or peroxynitrite by reducing thiols such as glutathione, thioredoxin, tryparedoxin, alkyl hydroperoxide reductase flavoprotein oxidoreductase component (AhpF) (Seo *et al*, 2000 and Dubuisson *et al*, 2004).

Six PRDX isoforms have been found in mammals, which can be divided into three classes as typical 2-Cys, atypical 2-Cys and 1-Cys. These conserved cysteine residues are involved in peroxide reductase activity. Peroxiredoxin 5 (PRDX5) is the last discovered peroxidase widely distributed in the tissues of prokaryotes and eukaryotes, which locates in peroxisomes, mitochondria and cytosol (Seo *et al*, 2000). It has 162 amino acids with molecular weight of 17 kDa. PRDX5 belongs to the atypical 2-Cys class with an N-terminal cysteine (Cys47) and a C-terminal cysteine (Cys151) forming an intramolecular disulfide bond (Fig.1 (b)) (Declercq *et al*, 2001). Its structure is different from the typical 2-Cys PRDXs whose oxidized form was only stabilized by intermolecular disulfide bond (Smeets *et al*, 2008).



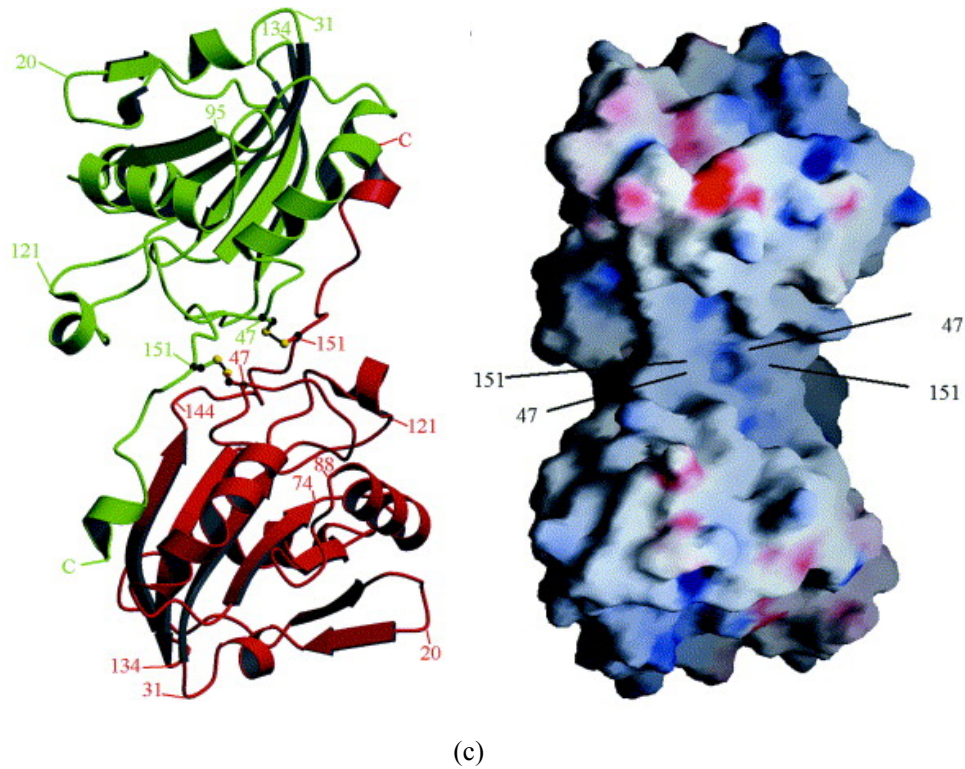


Fig.1 Structures of PRDX5. (a) Reduced form of PRDX5; (b) Oxidized form of PRDX5- Intramolecular disulfide bond; (c) Oxidized form of PRDX5- Two intermolecular disulfide bonds (Declercq *et al*, 2004)

2. PTS1 of human PRDX5

PRDX5 has a normal PTS sequence as –SQL. However, the interaction with Pex5p cannot be observed *in vitro*. This is probably because the N-terminus of PRDX5 is buried in a helix structure as shown in Fig.2. Moreover, the Gln at -2 position forms strong hydrogen bonds with the Asn at 142 position, making the PTS1 unavailable to Pex5p.

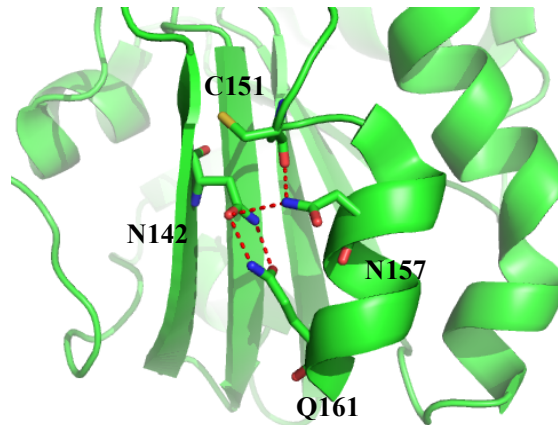


Fig.2 The intra-molecular interaction within PTS1 region of PRDX5

It was found in the previous studies that this Asn could be very important for the PRDX5 structure in both monomer and dimer, and PRDX5 do not bind to Pex5p when it is mutated to alanine (Fodor, unpublished). The aim of this project is to try to free up the PTS1 by making three mutants: N157A, Q161K and C47S/N142A/C151S/N157A, and study their binding affinity with Pex5p.

1 μ l *DpnI* was added into the PCR products and incubated at 37 for 1 hour to digest the parental DNA. Then the *DpnI* treated DNA was transformed to DH5 α by heat shock methods, after incubating the amplified vectors were extracted from the cells by the miniprep kit and sent to Eurofins MWG GmbH for sequencing.

2. Over expression and purification

The PRDX5 mutant gene was inserted in the pETM-11 vector (Fig.3). The transformation, expression and purification steps were the same as AGT mutant described in 1.2-1.4.

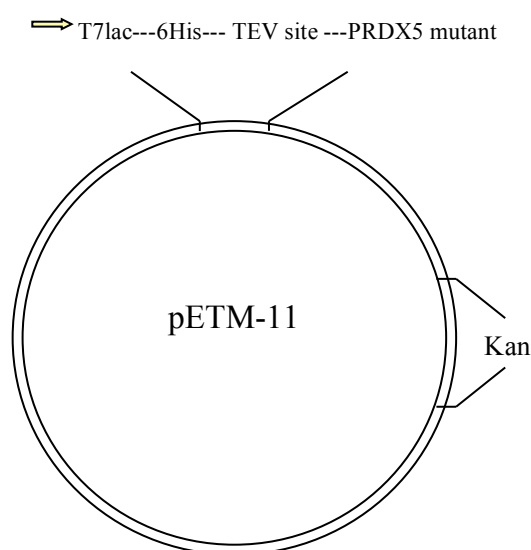


Fig.3. pETM-11 vector

3. GST-pull down

The binding ability of the purified mutants- N157A, Q161K and C47S/N142A/C151S/N157A as well as the wildtype PRDX5 to the Pex5p were detected by GST-pull down experiment. The process was the same as described in AGT part (PartA.3).

4. Size exclusion chromatography coupled with static light scattering

An analytical column filled with Sephadex-200 coupled with Static Light Scattering (SLS) was used for Q161K-Pex5p complex detection, to determine the MW of the

complex in solution.

5mg/ml Q161K and 6mg/ml Pex5p (about 3:2 molar ratio) were prepared and mixed in 1:1 volume ratio to make the Q161K-Pex5p complex with 5.5mg/ml concentration. After being filtered using 45 μ m filter by centrifuging for 2min at 7000rpm, 100 μ l complex and 100 μ l pure Q161K were injected into the Sephadex-200 analytic column respectively. The flow rate for elution was set as 0.8ml/min and the fractions were collected in a 96-well plate with 0.8ml liquid per well. After gel filtration, the fractions from Q161K-Pex5p complex were loaded to a 12% SDS-PAGE gel followed by electrophoresis. The molecular weights of Q161K and the complex were measured by SLS.

5. High-throughput crystallization of the Pex5p-Q161K complex

In order to find out suitable crystallization conditions for the Pex5p-Q161K complex, a high-throughput crystallization method was used for the initial screening by the HTX lab at the EMBL-Hamburg outstation.

6. ITC experiments

To analyze the monomer-dimer equilibrium, about 0.22 mM of Q161K, N157A and C47S/N142A/C151S/N157A were titrated into the stirred calorimeter cell (25) initially containing 1.4 ml buffer with 10 μ l per injection. The endothermic heat pulses generated from monomerization were measured. We also used ITC to detect the binding affinity of Pex5p and Q161K with the identical steps described in PartA.6.

Results

1.Quick change mutagenesis

For the control plates without growing colony, the mutagenesis rates of each mutant (N157A and Q161K) were determined as 100%. And the sequences of both mutants were correct (Fig.4 and Fig.5)

1	MAPIKVGD AIPAVEVFEGEPGNKVNLAELFKGKKGV LFGVPGAFTPGCSKTHLPGFVEQA	60 Query
1	MAPIKVGD AIPAVEVFEGEPGNKVNLAELFKGKKGV LFGVPGAFTPGCSKTHLPGFVEQA	60 P30044-2
61	EALKAKGVQVVACL SVNDAFVTGEWGRAHKAEGKVRLADPTGAFGKETDLLLLDDSLVSI	120 Query
61	EALKAKGVQVVACL SVNDAFVTGEWGRAHKAEGKVRLADPTGAFGKETDLLLLDDSLVSI	120 P30044-2
121	FGNRRLKRF SMVVQDGI VKALNVEPDGTGLTCSLAPAIISQL	162 Query
121	FGNRRLKRF SMVVQDGI VKALNVEPDGTGLTCSLAP IISQL	162 P30044-2

Fig.4 The sequence alignment of N157A to the wildtype PRDX5

1	MAPIKVGD AIPAVEVFEGEPGNKVNLAELFKGKKGV LFGVPGAFTPGCSKTHLPGFVEQA	60 Query
1	MAPIKVGD AIPAVEVFEGEPGNKVNLAELFKGKKGV LFGVPGAFTPGCSKTHLPGFVEQA	60 P30044-2
61	EALKAKGVQVVACL SVNDAFVTGEWGRAHKAEGKVRLADPTGAFGKETDLLLLDDSLVSI	120 Query
61	EALKAKGVQVVACL SVNDAFVTGEWGRAHKAEGKVRLADPTGAFGKETDLLLLDDSLVSI	120 P30044-2
121	FGNRRLKRF SMVVQDGI VKALNVEPDGTGLTCSLAPNIISKL	162 Query
121	FGNRRLKRF SMVVQDGI VKALNVEPDGTGLTCSLAPNIIS+L	162 P30044-2

Fig.5 The sequence alignment of Q161K to the wildtype PRDX5

2.GST pull down

According to the SDS-PAGE gel shown in Fig.6, it was confirmed that Pex5p and wildtype PRDX5 could not interact *in vitro*, and the C47S/N142A/C151S/N157A mutant could not bind to Pex5p as well. However, we found that Q161K and N157A were able to bind to Pex5p, demonstrating obvious bands at the 17 kDa position. Then the Q161K with the strongest positive signal was selected for the further studies.

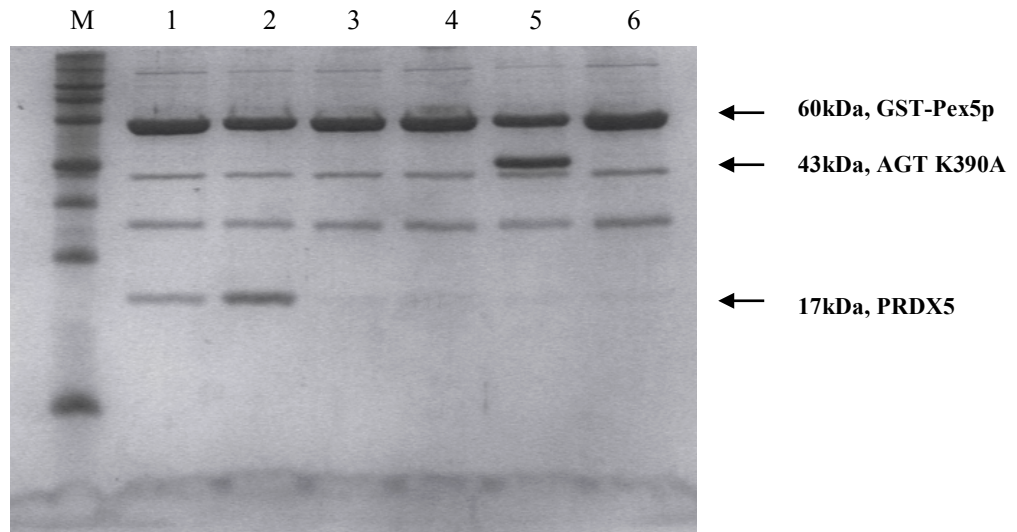


Fig.6 SDS-PAGE gel for GST-pull down experiment. 1-N157A; 2-Q161K; 3-C47S/N142A/C151S/N157A; 4- wildtype PRDX5; 5- positive control (AGT K390A); 6- negative control (Pex19p).

3. SLS experiment

The SLS spectrum for each single measurement was shown together in Fig.7. The measured molecular weight of Q161K was about 32.5 kDa, and the one of Q161K-Pex5p complex was 71.0 kDa. Based on the data in Table.2, it was suggested that Q161K in the solution was dimeric, and two Q161K monomers bound to one Pex5p molecule.

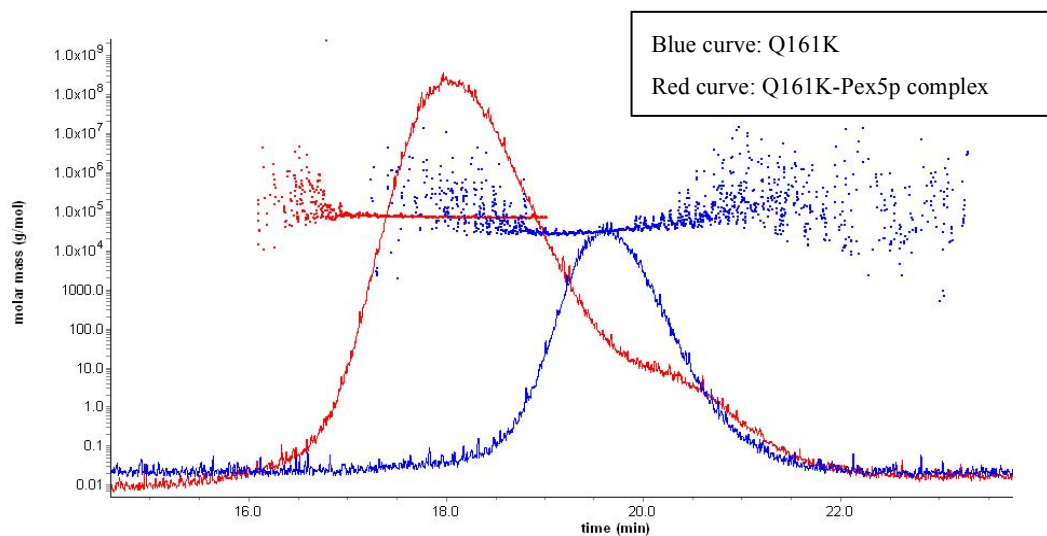


Fig.7 SLS spectrum of Q161K and Q161K-Pex5p complex

Table.2 Measured molecular weights by SLS

	Mw (Calculated)	Mw (Measured)
Q161K	17*2 kDa (dimer)	32.5 kDa (15%)
Pex5p-Q161K	102 kDa (17*2+36*2, if 1:1 molar ratio)	71.0 kDa (8%) (17*2+36)

For the Q161K-Pex5p mixture sample which showed a single peak (Fig.7, the red curve), the fractions (0.8ml/well) from gel filtration were tested by SDS-PAGE (Fig.8). Two bands at 17 kDa and 36 kDa positions which stand for Q161K and Pex5p were present in the SDS-PAGE gel, confirming the presence of the complex.

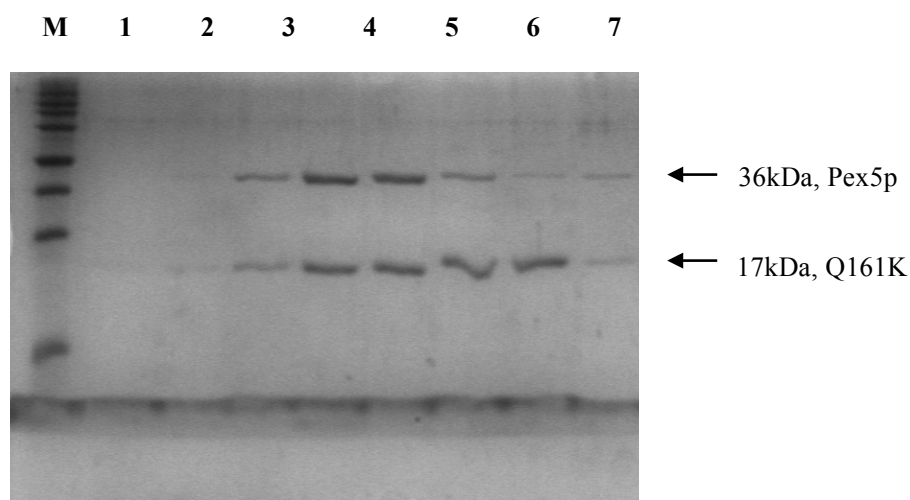


Fig.8 SDS-PAGE gel of the fragments from gel filtration of Q161K-Pex5p complex. 1-8: The fragments during ca.16min-22min as shown in Fig.7.

However, when the GST-Pex5p fusion protein was used as the receptor for Q161K, the measured molecular weight of GST-Pex5p and Q161K complex suggested a 1:1 molar ratio binding (Fig.9 and Table.3), which contradicted to the finding from the SLS experiment of Pex5p and Q161K.

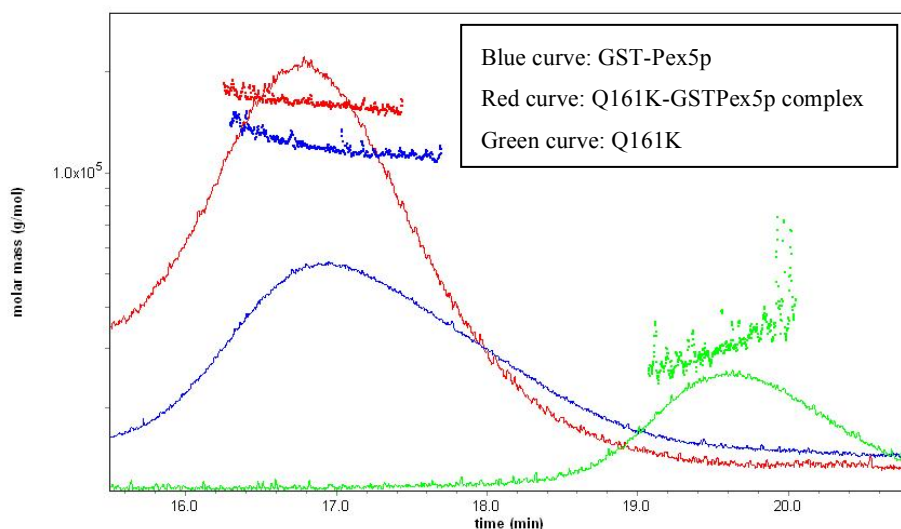


Fig.9. SLS spectrum of Q161K and Q161K-GST Pex5p complex

Table.3 Measured molecular weights by SLS

	Mw (Calculated)	Mw (Measured)
GST-Pex5p	122 kDa (dimer)	119.6 kDa (8%)
Q161K	34 kDa (dimer)	32.5 kDa (15%)
GST-Pex5p-Q161K	156 kDa (if 1:1 molar ratio binding)	162.8 kDa (9%)

4. ITC experiment

ITC dilution experiment of Q161K was performed to determine the thermodynamic parameters of monomerization. The critical transient concentration was found after about seven injections (10 μ l/inj) of 0.23 mM Q161K into the cell containing 1.4ml buffer initially. This can be seen in Fig.9(a). The critical transient concentration was roughly calculated as 9.9 μ M.

When the buffer was injected from the syringe into 0.023mM Q161K, the exothermic reaction could also be observed (Fig.10(b)), which could mean that the monomer-dimer equilibrium of PRDX5 is so sensitive that even minor changes in the molecule's environment might lead to changes in the oligomeric state.

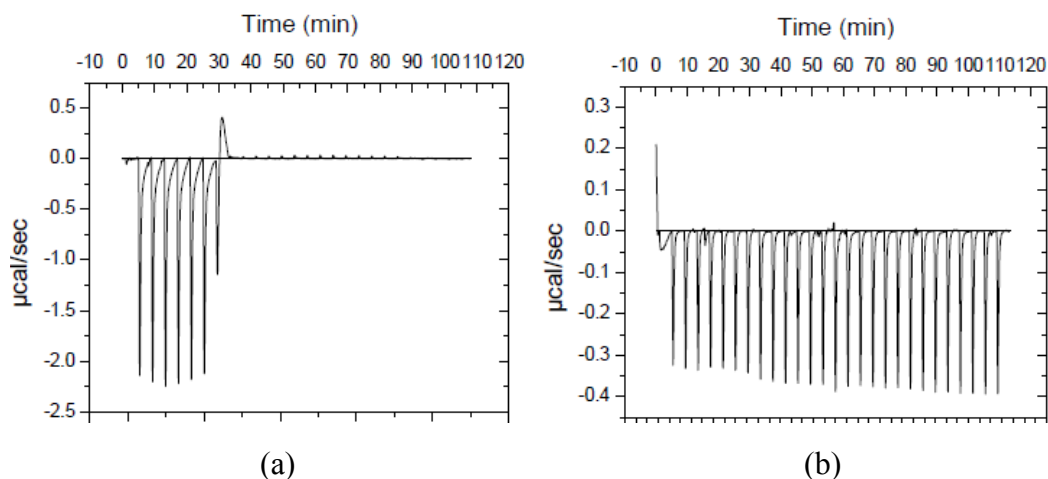


Fig.10 ITC dilution experiment of Q161K. (a) 0.23mM Q161K injected into buffer; (b) buffer injected into 0.023mM Q161K

In the case when 0.23mM Q161K was titrated into 0.023mM Pex5p, the value of critical transient concentration became double. It happened after fourteen injections when Q161K and Pex5p in the cell has 1:1 molar ratio (Fig.11(a)). When the concentrated Pex5p was injected into Q161K in the cell, a typical ITC curve could be seen as shown in Fig.11(b). However, after several repeated measurements (Fig.12 shows a couple of examples, others can be seen in appendix II), the measured thermodynamic parameters (the stoichiometry, ΔH , etc) were unstable.

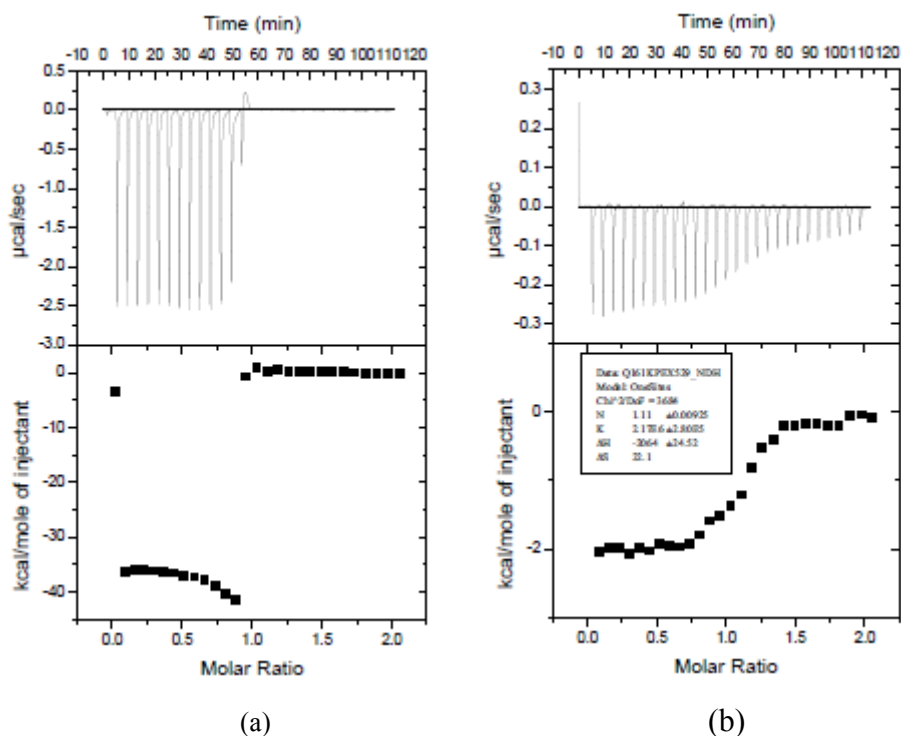


Fig.11 ITC of Q161K and Pex5p interaction. (a) 0.23mM Q161K injected to buffer; (b) 0.23mM Pex5p injected to 0.023mM Q161K.

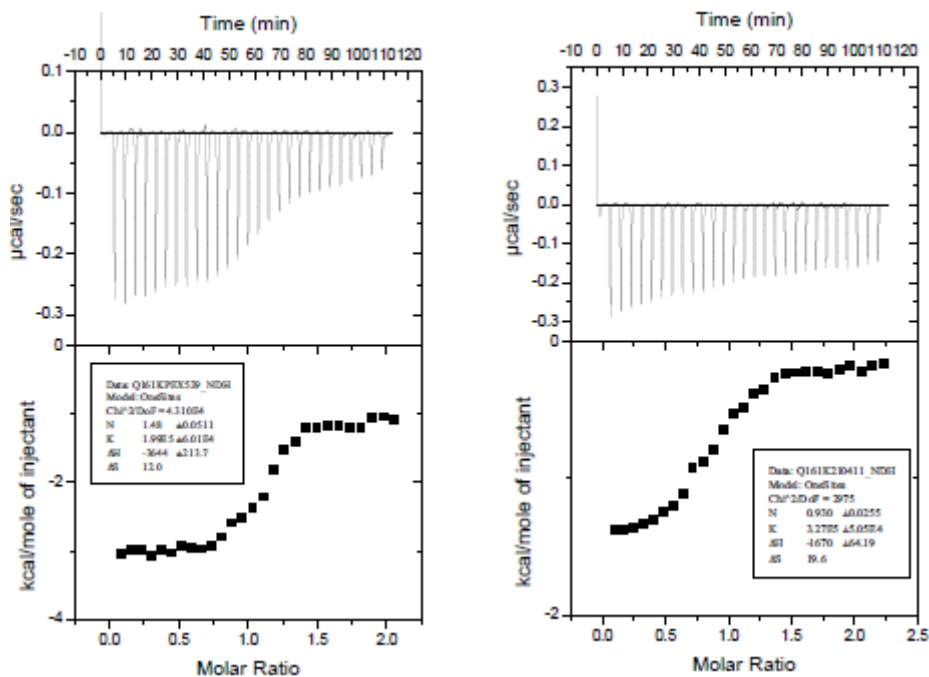


Fig.12 ITC experiments of Pex5p injected into Q161K

The N157A and the C47S/N142A/C151S/N157A was injected into the buffer as well. As a result, the N157A also demonstrated the critical transient concentration as Q161K (Fig.13(a)), whereas the C47S/N142A/C151S/N157A mutant did not perform the exothermic reaction (Fig.13(b)). It indicates that the disruption of the intermolecular interface by mutating cysteine to alanine may lead to exclusively monomeric PRDX5.

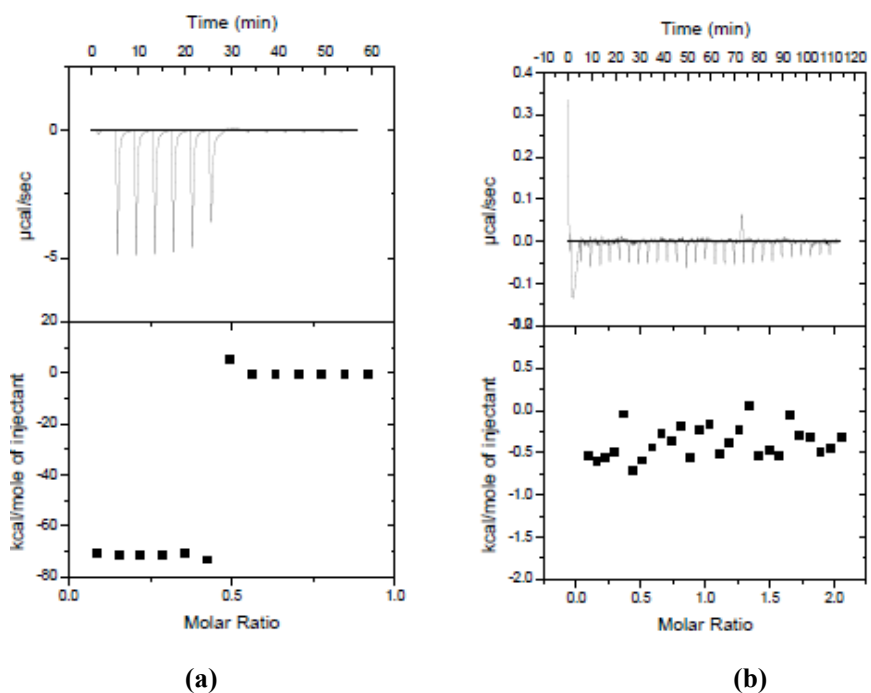


Fig.13 ITC dilution experiment. (a)N157A; (b) C47S/N142A/C151S/N157A.

5. High-throughput screening of crystallization condition

Unfortunately, there were no crystals growing under the test conditions.

Discussion

Three PRDX5 mutants: N157A, Q161K and C47S/N142A/C151S/N157A were constructed and purified. When the Gln was mutated to Lys, the binding to Pex5p was observed by GST pull down, and was confirmed by the further experiments such as SLS and ITC. Unfortunately, we cannot explain the binding mechanism due to the failure to crystallize the Q161K-Pex5p complex.

The ITC dilution experiments reveal a critical transient concentration (about 0.01mM) for the Q161K. The similar phenomenon was found in the classical 2-cysteine peroxoredoxins from *Homo sapiens*, *Arabidopsis thaliana*, and *Pisum sativum* (Barranco-Medina *et al*, 2008). The value of the critical transient concentration became double when the same Q161K sample was injected into the Pex5p. This could mean that it was the monomer form of PRDX5 binding to Pex5p. The binding energy was not visible, because it was covered by the energy change of the PRDX5 monomerization. The critical concentration was reached seven injections later in presence of Pex5p, because the amount of free monomers was lower due to the binding to Pex5p. However, when the equilibrium was reached, there was no more PRDX5 monomerization, therefore no more binding events. This is why no more peaks were observed after the half titration. The other measurements were good because PRDX5 monomers were present, since we were closer to the critical concentration. However, the repeatability of the measurement was limited due the complexity of the reaction. The disruption of inter/intra-molecular disulphide bonds by mutating C to S made PRDX5 monomer, therefore the signals could not be observed.

The data indicates that the interaction of PRDX5 and Pex5p cannot happen passively, because the structure of PRDX5 is rather compact and there are many interactions in both the monomer and the dimer which involve the PTS1, therefore it should first be made available for binding. Whether this facilitator molecule is Pex5p alone, or there is another, yet to be characterized molecule, remains to be seen. The future direction of this study would be to focus on crystallization of the Q161K-Pex5p complex to get a clear view of the 3D structure. Besides, a triple-mutant C47S/C151S/Q161K can be constructed for the ITC experiment.

Reference

Barranco-Medina S., Kakorin S., Lazaro J. and Dietz K., Thermodynamics of the dimer-decamer transition of reduced human and plant 2-Cys peroxiredoxin, *Biochemistry*, 47 (2008), pp. 7196–7204.

Calzi M.L. and Poole L.B., Requirement for the two AhpF cystine disulfide centers in catalysis of peroxide reduction by alkyl hydroperoxide reductase, *Biochemistry* 36 (1997), pp. 13357–13364.

Declercq J.P., Evrard C., Clippe A., Stricht D.V., Bernard A. and Knoops B., Crystal structure of human peroxiredoxin 5, a novel type of mammalian peroxiredoxin at 1.5 Å resolution, *Journal of Molecular Biology*, 311 (2001), pp. 751-759.

Dubuisson M., Stricht D.V., Clippe A., Etienne F., Nauser T., Kissner R., Koppenol W.H., Rees J.F., Knoops B., Human peroxiredoxin5 is a peroxynitrite reductase, *FEBS Letters*, 571 (2004), pp. 161–165.

Hofmann B., Hecht H.J. and Flohé L., Peroxiredoxins, *Biol. Chem.* 383 (2002), pp. 347–364.

Lee P.S., Hwang Y.S., Kim Y.J., Kwon K., Kim H.J., Kim K. and Cha H.J., Cyclophilin A binds to peroxiredoxins and activates its peroxidase activity, *J. Biol. Chem.* 276 (2001), pp. 29826–29832.

Rhee S.G., Kang S.W., Chang T.S., Jeong W. and Kim K., Peroxiredoxins, a novel family of peroxidases, *IUBMB Life*, 52 (2001), pp. 35–41.

Seo M.S., Kang S.W., Kim K., Baines I.C., Lee T.H. and Rhee S.G., Identification of a new type of mammalian peroxiredoxin that forms an intramolecular disulfide as a reaction intermediate, *J. Biol. Chem.* 275 (2000), pp. 20346–20354.

Smeets A., Marchand C., Linard D., Knoops B. and Declercq J.P., The crystal structures of oxidized forms of human peroxiredoxin 5 with an intramolecular disulfide bond confirm the proposed enzymatic mechanism for atypical 2-Cys peroxiredoxins, *Archives of Biochemistry and Biophysics*, 477 (2008), pp. 98-104.

Conclusion

In order to find out what are the structural and conformational requirements for successful cargo recognition, two model proteins were used. One is human alanine-glyoxylate aminotransferase (AGT), which has a non consensus PTS1 sequence: KKL. The other one is Peroxiredoxin 5 (PRDX5), whose buried PTS1 structure is inaccessible to Pex5p *in vitro*.

With the AGT mutants, it is known from this project what is the PTS1 dependence of receptor binding. The mutation of -3 position lysine to alanine can lead to a large increase of binding affinity to Pex5p, whereas the mutation of the -2 position lysine to alanine results in the complete loss of binding ability. Besides, AGT binds pex5p as a dimer. It is also revealed that the Pex5p TPR domain is flexible enough to adapt to various cargoes with different PTS1 sequence.

While in the case of PRDX5, it seems that monomerization is a prerequisite of successful binding, and moreover, possibly the conformation of the protein should also be Pex5p-binding competent, because the -2 position glutamine to lysine mutation is necessary.

Acknowledgement

I would like to express my gratitude to our group leader Matthias Wilmanns for giving me an opportunity to work in his group in EMBL, Hamburg Outstation, and for his generous financial support for my living in the beautiful Hamburg city.

Meanwhile I would like to thank my supervisor Krisztian Fodor for providing this well designed project and the great supervising. I also would like to thank him for helping me correct my report and for all other things. I will never forget the happiness when we discovered new results and the frustration when we suffered from ITC nightmare.

I am also immensely thankful to my examiner -Prof. Joakim Norbeck for evaluating my work and thesis, and organizing my thesis defense.

Finally I want to thank Florian Sauer, who always encouraged me to overcome the difficulties, and thank all the EMBL wetlab staff for the kind helps.

Appendix I Buffers and solutions

Buffer A 1L:

50mM HEPES pH7.5, 150mM NaCl, 50mM Imidazole, 2mM BME
MiliQ till 1L.

Buffer B 1L:

50mM HEPES pH7.5, 150mM NaCl, 500mM Imidazole, 2mM BME
MiliQ till 1L.

Gel filtration buffer 1L:

50mM HEPES pH7.5, 150mM NaCl, 2mM BME
MiliQ till 1L.

1 M Sodium Phosphate Buffer, pH 8.0, 100ml (for the CD measurement):

1 M Na₂HPO₄, 93.2 ml

1 M NaH₂PO₄, 6.8 ml

Mix together.

Appendix II ITC figures

1. Dissociation constant of AGT mutants at 25°C (μM)

	Q385A	P388A	K389A	K390A	K391A	K390A/K391A
1	6.99	1.69	6.45	0.36	-	5.18
2	11.1	1.63	3.80	0.20	-	4.20
3	5.41	2.35	8.62	0.39	-	5.78
AV	7.83	1.89	6.29	0.32	-	5.05

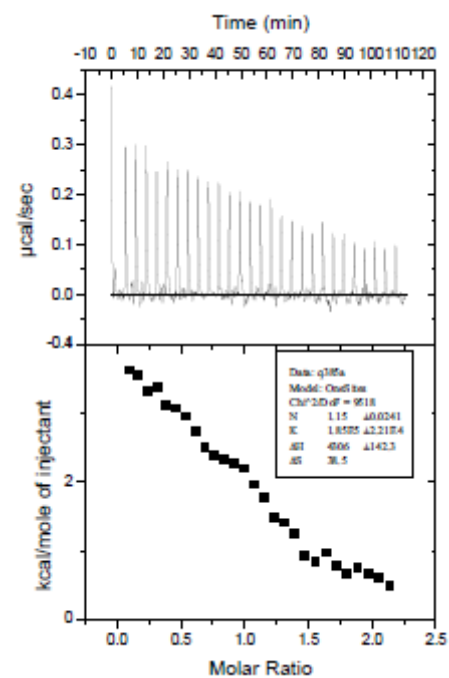
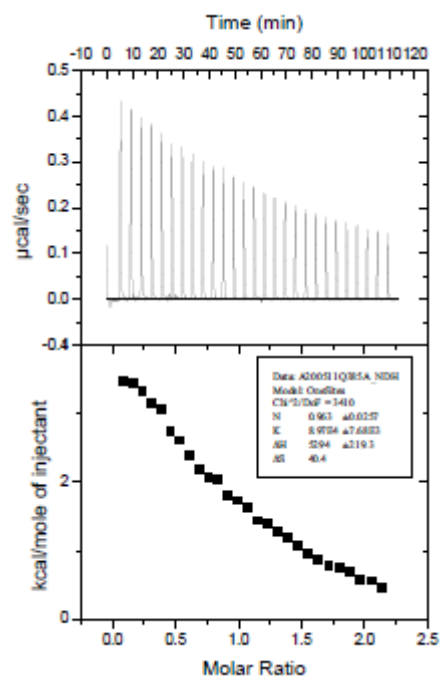
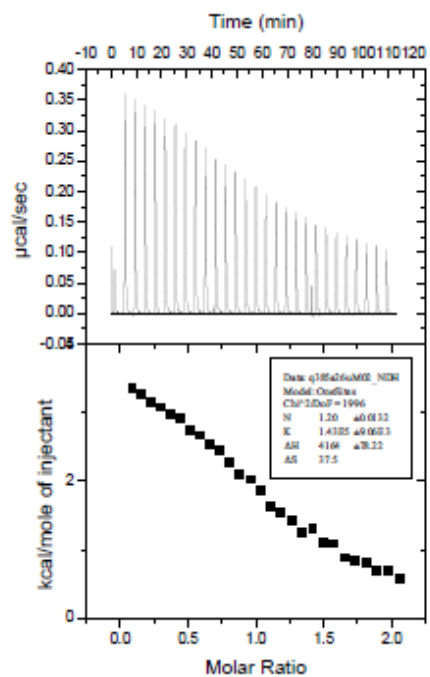
2. ΔH of AGT mutants at 25°C (cal/mol)

	Q385A	P388A	K389A	K390A	K391A	K390A/K391A
1	4164	3387	1288	3189	-	2027
2	5294	4660	1052	2444	-	3153
3	4306	3892	1475	2863	-	1949
AV	4588	3979	1271	2832	-	2376

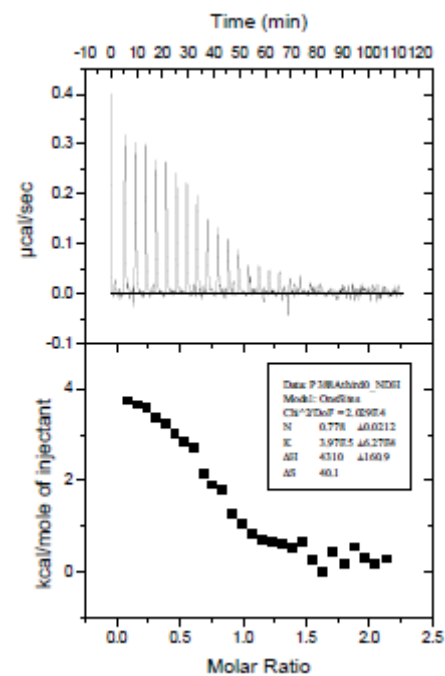
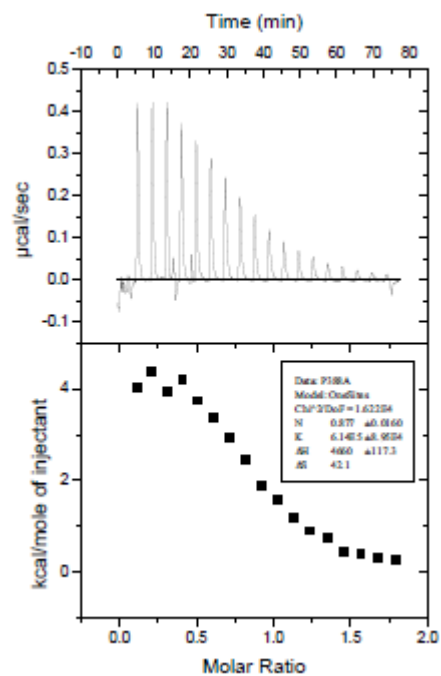
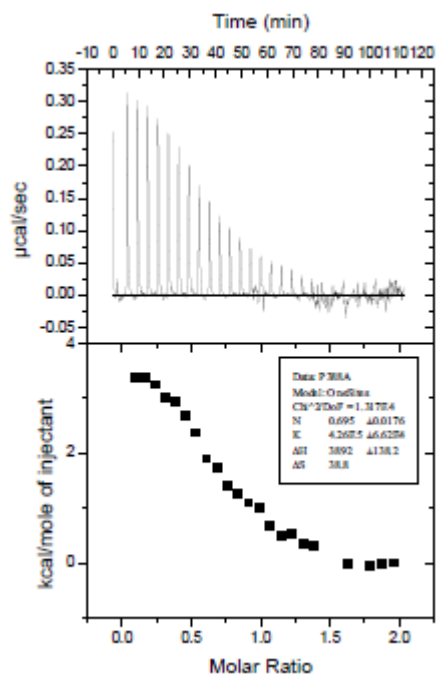
3. ΔS of AGT mutants at 25°C (cal/mol·K)

	Q385A	P388A	K389A	K390A	K391A	K390A/K391A
1	37.5	37.8	28.1	40.2	-	31.0
2	40.4	42.1	28.3	38.9	-	35.2
3	38.5	38.8	28.1	38.9	-	30.5
AV	38.8	39.6	28.2	39.3	-	32.2

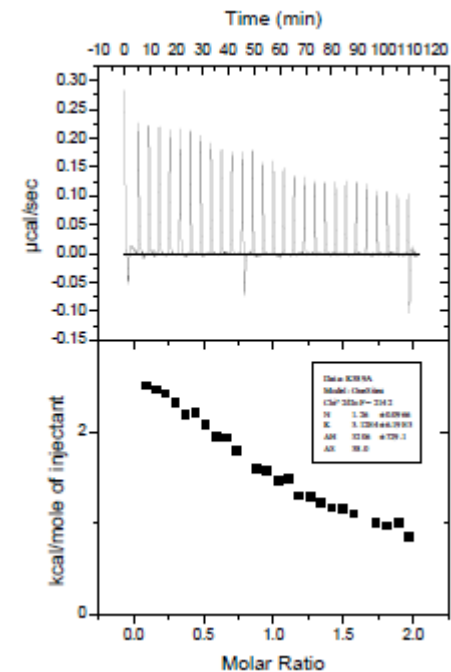
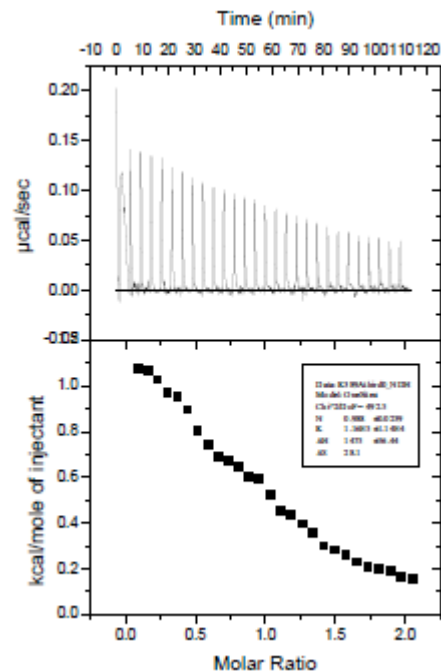
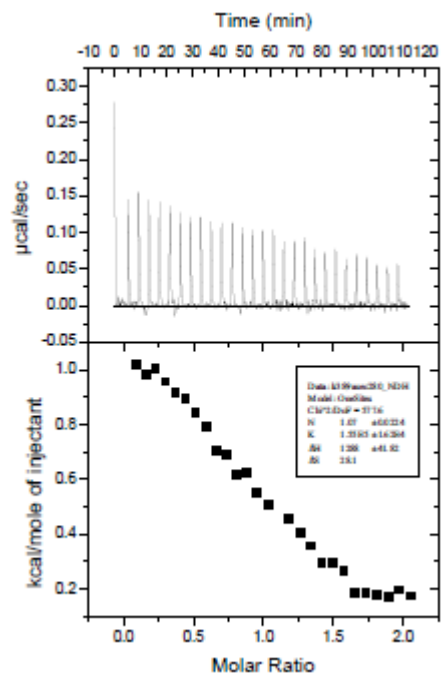
AGT Q385A:



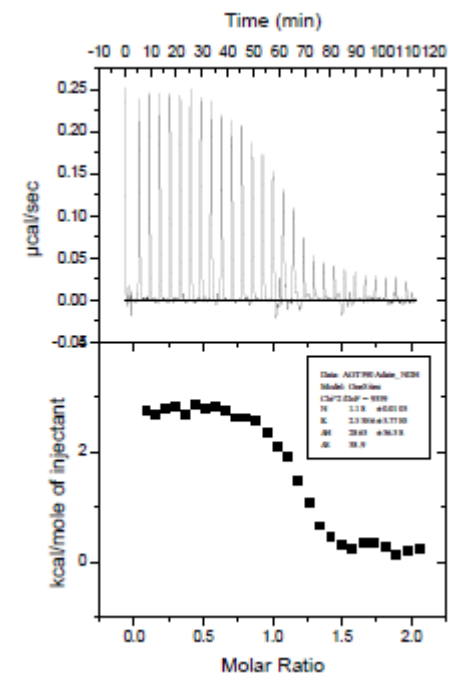
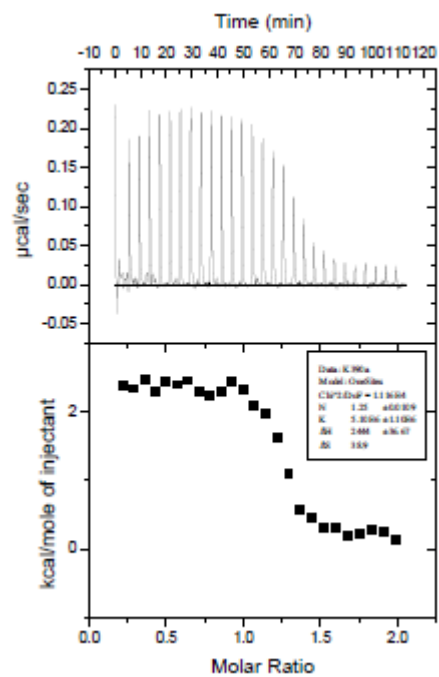
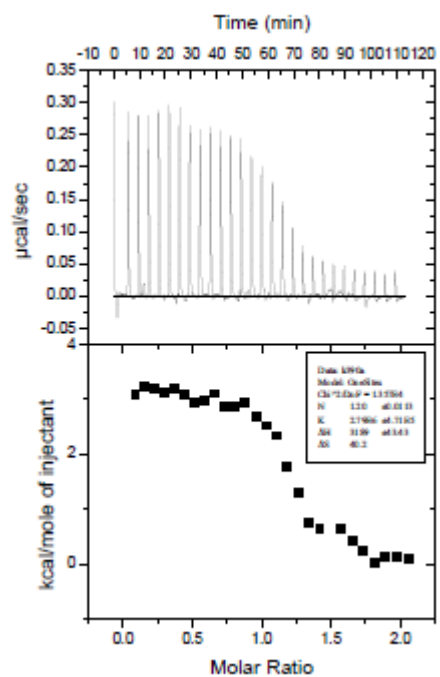
AGT P388A:



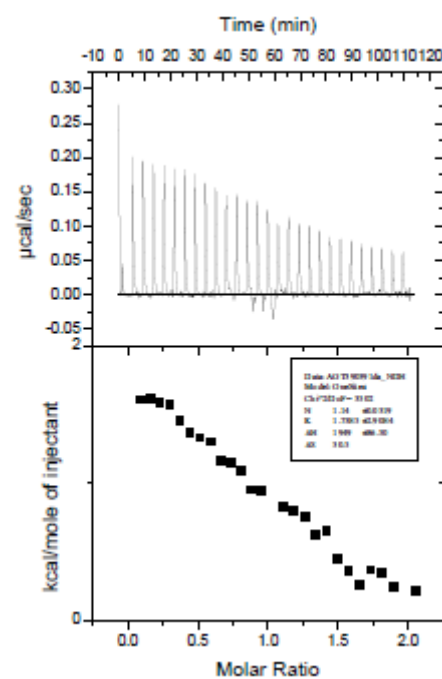
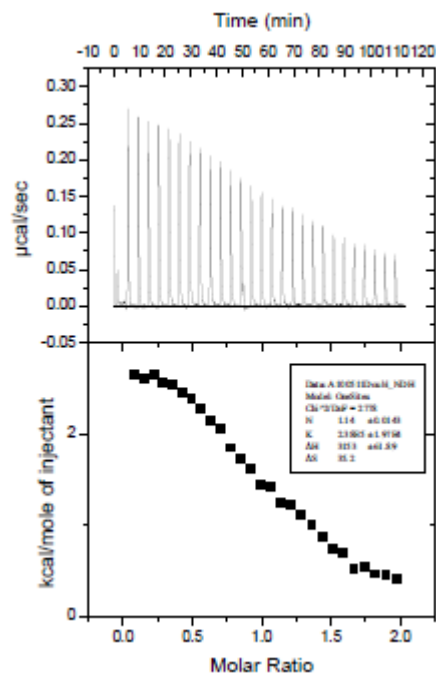
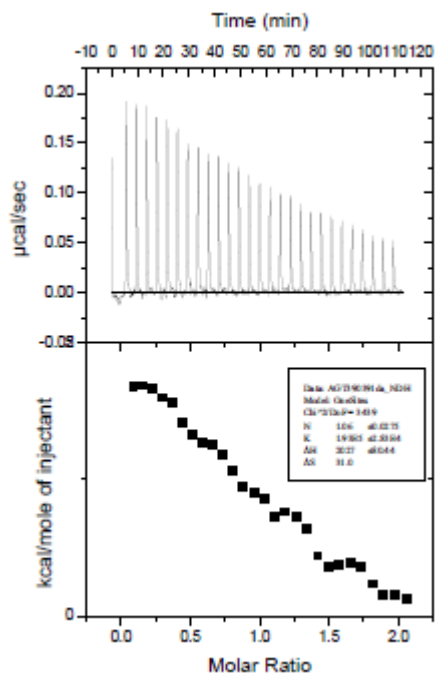
AGT K389A:



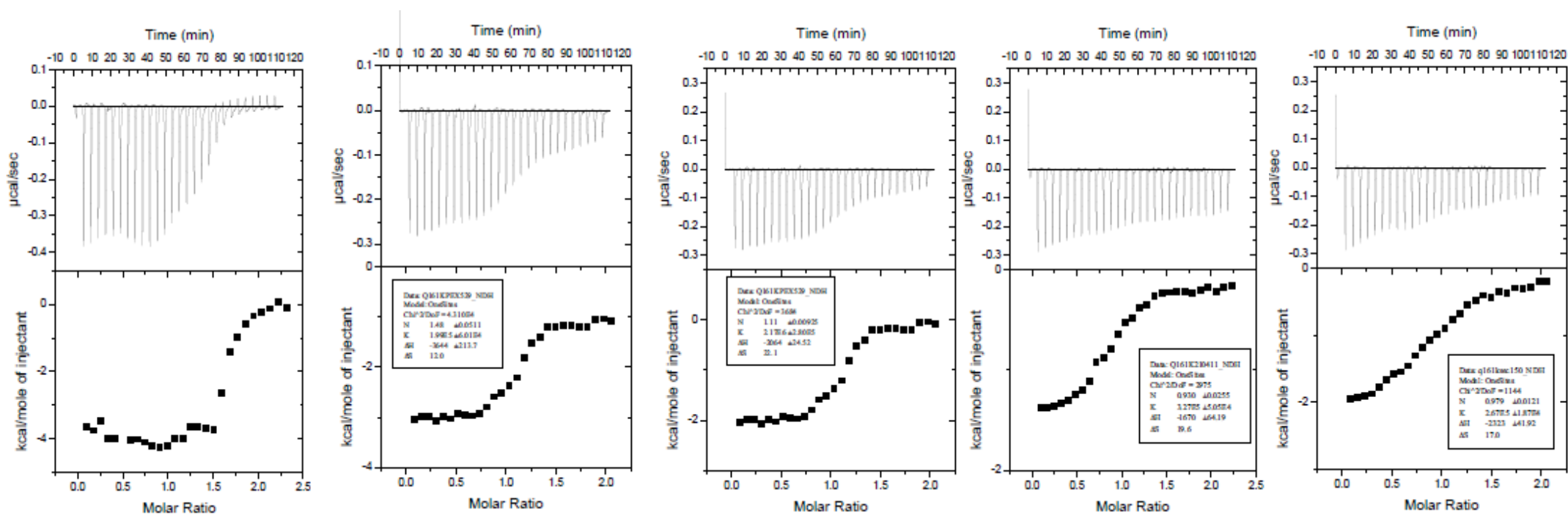
AGT K390A:



AGT K390A/K391A:



PRDX5 Q161K:



* The repeatability is low.